RESEARCH ARTICLE

REVISED Engineering the thin film characteristics for optimal performance of superconducting kinetic inductance amplifiers using a rigorous modelling technique [version 2; peer review: 3 approved]

Boon-Kok Tan[1], Faouzi Boussaha[2], Christine Chaumont[2], Joseph Longden[1], Javier Navarro Montilla[1]

[1]Department of Physics (Astrophysics), University of Oxford, Denys Wilkinson Building, Keble Road, Oxford, OX1 3RH, UK
[2]GEPI (CNRS UMR 8111), Observatoire de Paris, PSL Université, Paris, France

v2 **First published:** 19 Jul 2022, **2**:88
https://doi.org/10.12688/openreseurope.14860.1
Latest published: 13 Sep 2023, **2**:88
https://doi.org/10.12688/openreseurope.14860.2

Abstract

Background: Kinetic Inductance Travelling Wave Parametric Amplifiers (KITWPAs) are a variant of superconducting amplifier that can potentially achieve high gain with quantum-limited noise performance over broad bandwidth, which is important for many ultra-sensitive experiments. In this paper, we present a novel modelling technique that can better capture the electromagnetic behaviour of a KITWPA without the translation symmetry assumption, allowing us to flexibly explore the use of more complex transmission line structures and better predict their performance.
Methods: In order to design a KITWPA with optimal performance, we investigate the use of different superconducting thin film materials, and compare their pros and cons in forming a high-gain low-loss medium feasible for amplification. We establish that if the film thickness can be controlled precisely, the material used has less impact on the performance of the device, as long as it is topologically defect-free and operating within its superconducting regime. With this insight, we propose the use of Titanium Nitride (TiN) film for our KITWPA as its critical temperature can be easily altered to suit our applications. We further investigate the topological effect of different commonly used superconducting transmission line structures with the TiN film, including the effect of various non-conducting materials required to form the amplifier.
Results: Both of these comprehensive studies led us to two configurations of the KITWPA: 1) A low-loss 100 nm thick TiN coplanar waveguide amplifier, and 2) A compact 50 nm TiN inverted microstrip amplifier. We utilise the novel modelling technique described in the first part of the paper to explore and investigate the optimal design

Open Peer Review

Approval Status ✓ ✓ ✓

	1	2	3
version 2 (revision) 13 Sep 2023	✓ view	✓ view	✓ view
version 1 19 Jul 2022	? view	? view	? view

1. **Fausto Patricio Mena**, University of Chile, Santiago, Chile
National Radio Astronomy Observatory, Charlottesville, USA
2. **Wenlei Shan**, National Astronomical Observatory of Japan (NAOJ), Tokyo, Japan
3. **Martina Esposito**, SPIN Institute, Naples, Italy

Any reports and responses or comments on the article can be found at the end of the article.

and operational setup required to achieve high gain with the broadest bandwidth for both KITWPAs, including the effect of loss.
Conclusions: Finally, we conclude the paper with the actual layout and the predicted gain-bandwidth product of our KITWPAs.

Keywords
Parametric Amplifier, Travelling Waves, Kinetic Inductance, Superconducting Thin Films, Bardeen-Cooper-Schrieffer (BCS) Theory, Transmission Lines, Microwave, Quantum-Limited Noise

This article is included in the Horizon 2020 gateway.

This article is included in the European Research Council (ERC) gateway.

This article is included in the Materials Engineering gateway.

Corresponding author: Boon-Kok Tan (boonkok.tan@physics.ox.ac.uk)

Author roles: Tan BK: Conceptualization, Data Curation, Formal Analysis, Funding Acquisition, Investigation, Methodology, Project Administration, Software, Supervision, Validation, Visualization, Writing – Original Draft Preparation, Writing – Review & Editing; **Boussaha F**: Data Curation, Investigation, Resources, Supervision; **Chaumont C**: Data Curation, Investigation, Resources; **Longden J**: Investigation, Software, Visualization, Writing – Original Draft Preparation; **Navarro Montilla J**: Investigation, Writing – Original Draft Preparation

Competing interests: No competing interests were disclosed.

Grant information: This project has received funding from the European Research Council (ERC) under the European Union's Horizon 2020 research and innovation programme (grant agreement No 803862).
The funders had no role in study design, data collection and analysis, decision to publish, or preparation of the manuscript.

How to cite this article: Tan BK, Boussaha F, Chaumont C *et al.* **Engineering the thin film characteristics for optimal performance of superconducting kinetic inductance amplifiers using a rigorous modelling technique [version 2; peer review: 3 approved]** Open Research Europe 2023, **2**:88 https://doi.org/10.12688/openreseurope.14860.2

First published: 19 Jul 2022, **2**:88 https://doi.org/10.12688/openreseurope.14860.1

REVISED **Amendments from Version 1**

The manuscript was updated in response to the reviewers comments and suggestions, including correcting for all the typos and grammatical errors. Additional sentences were also added to clarify certain statements that were commented as unclear by the reviewers. A mistake on the unit of surface resistance has been updated to mΩ /□ instead of kΩ /□, hence Figure 2, Figure 3, Figure 5, Figure 6, Figure 7 and Figure 8 has been updated. Figure 10 & Figure 17 has also been updated with additional labelling to better explain the figures to the readers. Section 5.3 has been removed to shorten the manuscript as suggested by one of the reviewer. A new citation has been added "Valenzuela, D., Mena, F. P., & Baselmans, J. Modelling dielectric losses in microstrip traveling-wave kinetic-inductance parametric amplifiers. In 30th International Symposium on Space THz Technology (Gothenburg & Sweden, 2019) pp (pp. 63-66).", as requested by one of the reviewer. The assumption that $R \rightarrow 0$ and $G \rightarrow \infty$ has been replaced with $R << \omega L$ and $G << \omega C$.

Any further responses from the reviewers can be found at the end of the article

Plain language summary

A Kinetic Inductance Travelling Wave Parametric Amplifier (KITWPA) is a type of quantum amplifier developed recently that can potentially achieve high gain across broad bandwidth, with the lowest possible noise performance allowed by nature's fundamental limits. In this article, we describe a new modelling technique that allows us to better capture the complex behaviour of the various materials used to form the amplifier. It also provides us with the flexibility to explore the use of more complicated structures in our amplifier to enhance their performance. As the amplifier is formed using the superconducting thin film, we investigate the behaviour of different types of superconducting material to compare their pros and cons in terms of magnitude of inductance that gives rise to high gain, and surface residual resistance that could potentially increase losses. We found that the choice of superconductor used is not critical to the performance of the amplifier, as long as the thickness of the film can be adjusted and fabricated within the capability of modern photo-lithography techniques. We therefore select one of the superconducting materials, the titanium nitride (TiN) film with appropriate thickness, for developing our KITWPAs. We further investigate the suitable transmission line topology required to form the amplifier. We then make use of the new methodology developed earlier to search for the optimum combination of various design and operational parameters required to operate the amplifier, paying special attention to the effect of loss that may impact the performance of our amplifiers. Finally, we conclude the article with the actual design of two KITWPAs, as well as their predicted gain profiles centred around 8 GHz with close to 100% fractional bandwidth performance.

1 Introduction

Many ultra-sensitive experiments such as astronomical receivers, quantum computation platforms and axion-like dark matter search experiments require the use of low-noise amplifiers to boost the signal-to-noise ratio of the weak detected signal. Traditionally, the amplification is achieved using High Electron Mobility Transistor (HEMT) amplifiers or low-noise Josephson Parametric Amplifiers (JPAs). Although the semiconductor-based HEMT amplifiers can achieve broadband amplification[1–3], their noise performance is still far from approaching the quantum limit, and their heat dissipation is high, therefore limiting their deployment for large pixel count experiments due to the limited cryogenic cooling power capability. Whilst JPAs can achieve quantum noise performance, their operational bandwidth is relatively narrow at only a few percentage fractional bandwidth[4–6]. A travelling wave parametric amplifier (TWPA), on the other hand, can achieve similar high gain and low noise performance but with close to $2 - 3\times$ orders of magnitude wider bandwidth[7,8]. Their negligible heat dissipation and the ease of fabrication also makes them the preferred choice for large pixel count applications, such as enabling the construction of large millimetre-astronomical focal plane arrays[9–12] and large qubit-number quantum computers[13–16], and accelerating the searching speed of axion dark matter experiments[17–19].

The operation of a TWPAs is similar to that of a JPA. The amplification is realised by transferring the energy from an injected strong modulating tone to the weak detected signal through a wave mixing mechanism within a nonlinear medium. In order to increase the interaction time between the strong pump and the weak signal to attain high gain, JPAs generally confine the nonlinear medium within a resonant cavity, hence the amplification only occurs within a limited bandwidth dictated by the cavity. TWPAs achieve broadband amplification by unfolding the nonlinear medium into a long transmission wire, thereby lifting the limitation imposed by the cavity. The source of the wire's nonlinearity can be induced by either utilising the kinetic inductance of a superconducting wire (KITWPA)[7,16,20–28] or with a series of Josephson junctions (JTWPAs) embedded along the wire[8,29–35].

Generally, the nonlinear reactance of the superconducting wire is weaker than that of the Josephson junction, hence KITWPAs require a much longer transmission length and higher pump power to achieve the same gain as the JTWPA counterpart. Even though the surface resistance of a short superconducting wire is negligible, a high current travelling along a much longer line spanning several tens to hundreds of wavelengths could still introduce a non-negligible compounded resistive loss. This resistive heating causes the KITWPA to have a poorer transmission strength and inferior noise performance compared to the JTWPA. Therefore it is important to carefully engineer the characteristics of the superconducting wire to achieve the quantum-limited noise performance with high gain over a shorter transmission length.

Although several designs of KITWPA have already been reported in the literature[7,16,20–27], their choice of the thin film material used to form the superconducting wire and the topology of the transmission line are often not clearly clarified. They are most likely being dictated by the existing fabrication capabilities or from prior experience in the design of superconducting devices that require high kinetic inductance such as microwave kinetic inductance detectors (MKIDs). The lack of extensive investigation of the effect of using different materials and transmission line topologies therefore indicates that the performance of the KITWPA may not yet have been fully

optimised. Therefore, in this paper, we aim to explore the effect of the properties of different types of superconducting thin films and transmission line topologies on the performance of the KITWPA, in particular their impact on the gain and loss performance of the amplifier, and the limits where the amplifier may cease to operate due to high resistive loss. Based on these analyses, we present the designs of two optimal KITWPAs that can achieve low loss performance with the shortest possible transmission length. We show the gain-bandwidth performance of the KITWPAs predicted using a novel method we developed to rigorously simulate the performance of the amplifiers taking advantage of 3-D electromagnetic (*em*) simulators and the simplicity of coupled-mode equations taking into account losses and subtle *em* effects. We shall discuss this new method in detail in the subsequent sections.

2 Methods

A TWPA relies on the nonlinear behaviour of a transmission medium to mediate energy exchange between several different frequency components through a wave mixing process. Amplification can be achieved through varying the nonlinear reactance of the medium by applying a strong 'pump' current at frequency ω_p. If a weak signal at frequency ω_s is applied, under proper conditions, the time-varying reactance would transfer the power from the pump to the signal, thereby achieving amplification. In theory, because this mechanism relies purely on nonlinear reactance response, the dissipation can be made arbitrarily small and Johnson noise can be eliminated, allowing the quantum limit to be reached. During the mixing process, a third frequency component, the 'idler' at ω_i will be generated and amplified to preserve the total momentum of the system. To a good approximation, these nonlinear inductances vary quadratically with current, therefore enabling the provision of wave-mixing through the nonlinear relation between the inductance and the RF currents.

The parametric gain produced through wave-mixing can be calculated using the coupled-mode differential equations[36–38], and is governed primarily by the phase relation of the waves propagating down the line. The gain is maximised if the phases of all propagating waves including the idler are matched. Under this condition, the signal would grow exponentially with line length and pump power instead of quadratically. However, these superconducting nonlinear media are generally dispersive, therefore a major challenge in designing the TWPAs is the need for a dispersion control element that can phase-match all the waves propagating along the parametric gain medium. These phase-matching elements can be realised e.g., in the form of a series of shunt resonators coupled to the nonlinear transmission line termed the resonator phase-matching (RPM) scheme[8,31], or by making use of periodical loading elements along the transmission medium[7,28,34] to create multiple abrupt stopbands along the frequency axis. The wave vector near these regions diverge exponentially away from the otherwise linear dispersion relation, similar to those found in the photonic crystals or electrons in a periodic potential. By placing the pump near one of these divergence regions, the phase of the pump can be shifted to minimise the phase mismatch, and allow the maximum energy transfer from the pump to the signal. They can also be engineered such that the additional stopbands coincide with the frequency of the higher pump harmonics generated through self-modulation, hence prohibiting their propagation and prevent shock wave formation.

The parametric gain produced through wave-mixing in KITWPA can be described using a set of coupled mode equations. The nonlinear wave equation that governs the operation of the amplifier is given by:

$$\frac{\partial^2 I}{\partial z^2} = RGI + (LG + RC)\frac{\partial I}{\partial t} + C\frac{\partial}{\partial t}\left[L\frac{\partial I}{\partial t}\right] \tag{1}$$

where R, L, G and C are the resistance, inductance, conductance and capacitance per unit length, respectively, I the propagating tones and z the position along the transmission line.

The nonlinear inductance term can be approximated by a quadratic expansion[7,39] as $L(I) = L_0\,[1 + (I/I_0)^2]$, where L_0 is the intrinsic inductance and I_0 is the scale of nonlinearity related to the critical current value I_C of the film. The solution for Equation 1 can be obtained by assuming the propagating fields are comprised of a group of forward moving waves represented by $I(z,\ t) = \frac{1}{2}A_m(z)e^{(-\gamma_m z+\omega_m t)}$+c.c., where m=p,s,i corresponding to the pump, signal and idler wave respectively, $\gamma_m = \alpha_m + i\beta_m$ the complex propagation constant comprising the attenuation constant α and the wave vector β, A_m the slowly varying amplitudes of the waves, ω_m the angular frequencies and c.c. represents the complex conjugate terms. Here we assume an efficient suppression of the pump's harmonics via schemes that would be explained in later section, hence we ignore all the higher harmonic components in our calculation. For operation in the four wave mixing (4WM) regime, the relation between the pump, signal and idler is dictated by $2\omega_p = \omega_s + \omega_i$.

Substituting the propagating waves $I(z,\ t)$ into Equation 1, assuming that $\left|\frac{d^2A_m}{dz^2}\right| \ll \left|\gamma_m\frac{dA_m}{dz}\right|$, and $\left|\frac{dA_m}{dz}\right| \ll |\gamma_m A_m|$ 7, and collecting the terms that have the same frequency as the pump, signal and idler produces a set of coupled equations in the low-loss limit ($R << \omega L$ and $G << \omega C$):

$$\begin{aligned}
\gamma_p\frac{\partial A_p(z)}{\partial z} &= \frac{\beta_p^2}{8I_0^2}\Big[A_pA_pA_p^*e^{-2\alpha_p z} + 2A_pA_sA_s^*e^{-2\alpha_s z} \\
&\quad + 2A_pA_iA_i^*e^{-2\alpha_i z} + 2A_p^*A_sA_ie^{-(\alpha_s+\alpha_i)z}e^{\Delta_\beta z}\Big] \\
\gamma_s\frac{\partial A_s(z)}{\partial z} &= \frac{\beta_s^2}{8I_0^2}\Big[2A_pA_p^*A_se^{-2\alpha_p z} + A_sA_sA_s^*e^{-2\alpha_s z} \\
&\quad + 2A_sA_iA_i^*e^{-2\alpha_i z} + A_pA_pA_i^*e^{(-2\alpha_p+\alpha_s-\alpha_i)z}e^{-\Delta_\beta z}\Big] \\
\gamma_i\frac{\partial A_i(z)}{\partial z} &= \frac{\beta_i^2}{8I_0^2}\Big[2A_pA_p^*A_ie^{-2\alpha_p z} + 2A_sA_s^*A_ie^{-2\alpha_s z} \\
&\quad + A_iA_iA_i^*e^{-2\alpha_i z} + A_pA_pA_s^*e^{(-2\alpha_p-\alpha_s+\alpha_i)z}e^{-\Delta_\beta z}\Big]
\end{aligned} \tag{3}$$

where $\Delta_\beta = 2\beta_p - \beta_s - \beta_i$. This set of coupled differential equations can be solved numerically to probe the evolution of the wave amplitudes of the pump, signal and idler, hence the gain or attenuation of these waves along the transmission line. One can prove that under the undepleted pump assumption i.e., the pump amplitude remains unchanged throughout the transmission

length $A_p(z) = A_p(0)$ where $A_p(0)$ is the initial pump amplitude, the parametric gain $g = \frac{1}{2}\sqrt{\kappa_s \kappa_i - \Delta_\phi}$ is maximised when the total phase mismatch $\Delta_\phi = 2\phi_p - \phi_s - \phi_i + \Delta_\beta = 0$ where $\phi_p = \frac{\beta_p}{8I_0^2} A_p(0)^2$, $\phi_{s,i} = \frac{2\beta_{s,i}}{\beta_p}\phi_p$ and $\kappa_{s,i} = \frac{\phi_{s,i}}{2}$. Nevertheless, in all the analyses presented in the following, we do not include the assumption of undepleted pump to highlight the effect of the additional loss term α on the performance of the KITWPAs.

A KITWPA can also be designed to operate in the three wave mixing (3WM) regime by DC-biasing the nonlinear transmission line[20,23,40,41]. In this case, $\omega_p = \omega_s + \omega_i$, and the DC-biased 3WM coupled mode equation can be derived using the same procedure, given as:

$$\begin{aligned}
\gamma_p \frac{\partial A_p(z)}{\partial z} &= \frac{\beta_p^2}{8I_0^2}\Big[A_p A_p A_p^* e^{-2\alpha_p z} + 2A_p A_s A_s^* e^{-2\alpha_s z} \\
&\quad + 2A_p A_i A_i^* e^{-2\alpha_i z} + 4I_{dc}^2 A_p \\
&\quad + 4I_{dc} A_s A_i e^{-(\alpha_s+\alpha_i)z} e^{\Delta_{\beta 3} z}\Big] \\
\gamma_s \frac{\partial A_s(z)}{\partial z} &= \frac{\beta_s^2}{8I_0^2}\Big[2A_p A_p^* A_s e^{-2\alpha_p z} + A_s A_s A_s^* e^{-2\alpha_s z} \\
&\quad + 2A_s A_i A_i^* e^{-2\alpha_i z} + 4I_{dc}^2 A_s \\
&\quad + 4I_{dc} A_p A_i^* e^{(-\alpha_p+\alpha_s-\alpha_i)z} e^{-\Delta_{\beta 3} z}\Big] \\
\gamma_i \frac{\partial A_i(z)}{\partial z} &= \frac{\beta_i^2}{8I_0^2}\Big[2A_p A_p^* A_i e^{-2\alpha_p z} + 2A_s A_s^* A_i e^{-2\alpha_s z} \\
&\quad + A_i A_i A_i^* e^{-2\alpha_i z} + 4I_{dc}^2 A_s \\
&\quad + 4I_{dc} A_p A_s^* e^{(-\alpha_p-\alpha_s+\alpha_i)z} e^{-\Delta_{\beta 3} z}\Big]
\end{aligned} \tag{4}$$

where $\Delta_{\beta 3} = \beta_p - \beta_s - \beta_i$ and I_{dc} the DC-biased current. Similarly, the total phase mismatch can be obtained via $\Delta_\phi = \phi_p - \phi_s - \phi_i + \Delta_{\beta 3} \to 0$.

As can be seen from the frameworks described above, apart from the initial conditions e.g., the initial wave amplitudes and frequencies etc., the only unknown in the coupled mode equations is the frequency dependent complex propagation constant of the transmission line γ. This is the only parameter that relates directly to the physical superconducting transmission line (STL) itself (including geometries, substrates, dielectric layers etc.), and it captures all the information required to probe the evolution of the various tones propagating along the transmission length (z), including all the loss mechanisms via $\Re(\gamma) = \alpha$ and the frequency dependent dispersion relation through $\Im(\gamma) = \beta$. The propagation constant γ can be obtained theoretically using a reduced Kirchhoff equivalent circuit of a unit cell in the form of ABCD matrixes[24,36] or utilising the RLGC (Resistence-Inductance-Conductance-Capacitance) model[37,42] via the series resistance, series inductance, shunt conductance and shunt capacitance calculated using complex superconducting surface impedance, and relating these quantities to γ. The behaviour of the full KITWPA model is then simulated assuming a translation symmetry relation (via Floquet Theorem) by multiplying a number of repeated unit cells to form the long STL.

However, this approach neglects many subtle effects such as fringing fields and discontinuities that could arise from cascading hundreds of these unit cells and it can only be used for very simple transmission line geometries e.g., it would be complicated to simulate an actual transmission line such as a coplanar waveguide (CPW) with capacitive stubs or an inverted CPW realistically. Furthermore, the calculation is lengthy with various special assumptions required for different types of materials and geometries. Apart from this frequency domain approach, another way to simulate the KITWPA performance is via the finite-difference-time-domain (FDTD) technique, but FDTD solvers are time consuming with demanding computational requirements[24,36]. Similar to the frequency domain approach, FDTD also suffers from the inflexibility to incorporate various different types of transmission line model.

In order to circumvent these downsides, we could take advantage of the versatility of commercial circuit simulators such as the 3D *em* software packages Ansys High Frequency Structure Simulator®(HFSS), the 2.5-D Sonnet® package or Keysight's Advanced Design System® (ADS), to fully describe the physical layout of the unit cell. This approach is extremely flexible for obtaining γ to feed into the framework above for calculating the gain-bandwidth product of the entire KITWPA, since one could include almost any possible structures within the modelling environment. In our case, we focus on the use of Ansys software suites (Ansys®Electronics Desktop) which make use of the full Maxwell equations and finite element method to calculate the electromagnetic properties of a 3D structure, and we use the example of a periodically loaded KITWPA for explaining the simulation procedure below. Due to the complexity of Ansys®Electronics Desktop, there are no freely available alternative open-source software that can replace the full functionality of this *em* software to perform the same simulation (to our knowledge). Nevertheless, we have described the primary methodology behind the software and have provided the associated output data and analysis code. Please see *Software availability* for further information.

To emulate the actual behaviour of the thin film in the superconducting state in the *em* model, we first calculate the complex surface impedance of the thin film using the Mattis-Bardeen equation[43], taking into account the film's thickness, critical transition temperature (T_c), gap voltage (V_{gap}), normal resistivity (ρ_N) and the operational bath temperature (T_{bath}). We then assign an impedance boundary condition to a perfect conductor (PEC) modelled as the thin film, with the calculated frequency-dependent complex surface impedance values. We further include the substrate and dielectric characteristic e.g., the finite resistivity of substrate and dielectric loss tangent etc. in the *em* model as well as the more realistic topology of the KITWPA layout such as subtle effect of fringing field, radiative losses, discontinuities, geometric inductance and capacitance of the STL and many other *em* effects. Once the unit cell comprising the main transmission line and the loading sections is modelled, we cascade them using the transfer matrix approach via the dot product of the unit cell's ABCD matrix to finally obtain γ of the full KITWPA chip, as shown in Figure 1. Here, we can further improve the model accuracy by including the impedance transformer and the bonding pads at the two ends of the

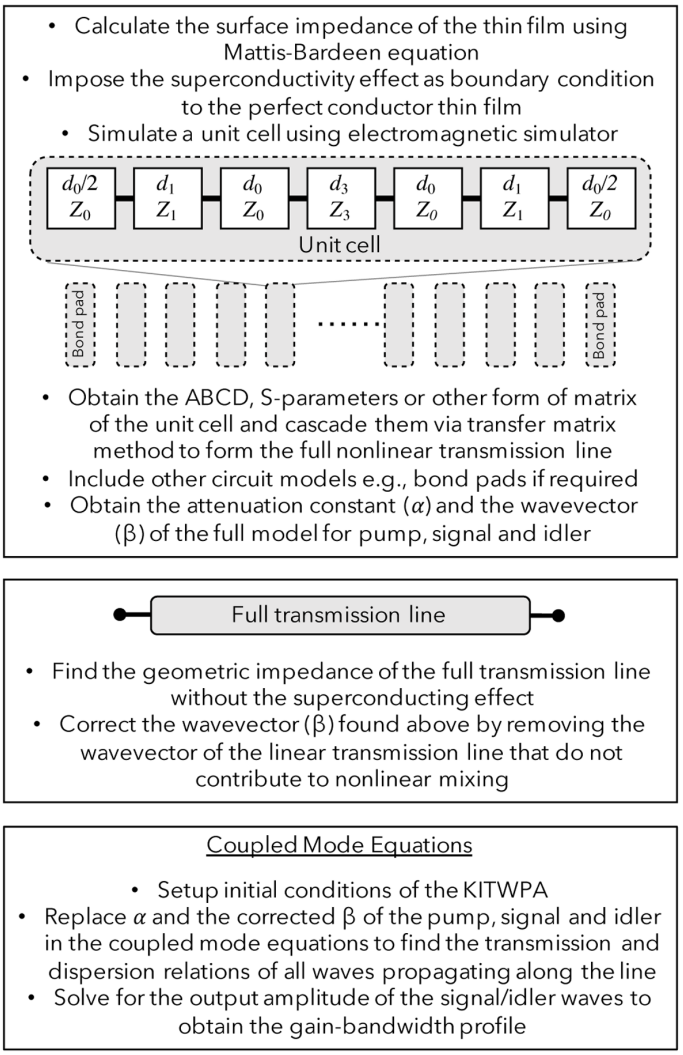

Figure 1. The sequence of computation procedures used to simulate the behaviour of the KITWPAs (Kinetic Inductance Travelling Wave Parametric Amplifiers), where $d_{0,1,3}$ and $Z_{0,1,3}$ is the length and characteristic impedance of the primary transmission line section, the first loading section and the third loading section, respectively.

amplifier chip. The obtained complex propagation constant is then injected into either Equation 2 or Equation 3 to probe the propagation behaviour of pump, signal and idler tones.

One distinct advantage of this methodology is that we combine the fast computation capability of the coupled mode equations with the commercial *em* software packages's ability to accurately capture the *em* behaviour of the KITWPA, therefore better predicts the performance of the amplifier. This method is powerful as it allows us to capture the true behaviour of the STLs, including small *em* effects which could become significant when designing a full KITWPA comprising hundreds of repeated unit cells. The flexibility offered by the *em* software also provides us with a fast and simple way to explore and analyse the behaviour of different variants of KITWPA, hence designing a bespoke KITWPA with optimal performance that suits to a particular application. It also offers fast, simple and easy way to explore more complex schemes such as the use of multi-layer superconductors[44] for future improvement of KITWPA, open up the possibility to include more complicated designs such as the incorporation of other circuit elements apart from the unit cell like filters, and potentially other functionality apart from amplification such as frequency converters[45].

It is important to note that unlike the conventional theoretical methods which assume the kinetic inductance of the thin film is dominating in the case of KITWPA and hence the geometric inductance (L_{geo}) of the STL is neglected in the calculation, our approach takes into account all the *em* behaviour of the STL, especially the geometric inductance that do not contribute to

the nonlinear mixing term described by L_0. Therefore, it is imperative to correct the wave vector β by removing the contribution from the L_{geo}, as shown in the second box of Figure 1.

3 Thin film characteristics

For the successful operation of a KITWPA, it is important to have a superconducting thin film which has the characteristic of high kinetic (surface) inductance (L_s), since the parametric gain is directly proportional to the inductance of the transmission line. This can be achieved by using high resistivity films such as Titanium (Ti), Niobium Titanium Nitride (NbTiN), or Niobium Nitride (NbN). However, it is commonly believed that high resistivity film would unavoidably incur high surface resistance (R_s) which could induce higher transmission loss, and potentially degrade the noise performance of the amplifier[46], preventing it from achieving the quantum limit. In this section, we explore the behaviour of several commonly used Bardeen–Cooper–Schrieffer (BCS) superconducting thin films to investigate if there is a potential solution for achieving high surface inductance (hence high gain) while keeping the surface resistance level under control (hence minimising transmission loss and added noise). As presented in Section 2, we calculate L_s and R_s using the Mattis-Bardeen equation. Apart from the three films stated above, we include low gap superconducting Aluminium (Al) and Niobium (Nb) for comparison, and Titanium Nitride (TiN) as the film's properties such as its gap voltage can be altered by controlling the Nitrogen flow rate during film deposition. Although our studies focus mainly on the application to KITWPA, the same analysis can be useful to other applications requiring high kinetic inductance with low resistive loss films as well, such as MKIDs. In the following analysis, we assume a KITWPA operating around 10 GHz at 10 mK.

Table 1 shows the various superconducting materials and their related properties under investigation in this paper, and Figure 2 shows the frequency dependency relation of the surface resistance R_s and the surface inductance L_s of various 50nm thick films under study. It is obvious from the plot that R_s increases quadratically with frequency well below the gap frequency (f_{gap}), while L_s remains considerably constant across the same range. This is important as different material exhibits different rate of increase in R_s which is directly related to the resistivity ρ_N. For example, NbN is shown to have much higher resistive loss with lower L_s compared to Ti at the same fractional frequency. From the plot, it clearly indicates that Ti would be the favourable film for KITWPA as it has the highest L_s and lowest R_s value (apart from Al and Nb). However, this could be misleading as the gap frequency of Ti under study here is approximately 41 GHz, whereas NbN has a gap frequency almost two order of magnitude higher. In this case, if we assume a KITWPA operating in the vicinity of 10 GHz, Ti film will be operating at $0.24\times f_{gap}$ while NbN closer to $0.01\times f_{gap}$. Referring back to Figure 2, one can immediately see that the R_s value for NbN is in fact much lower than Ti at $0.01\times f_{gap}$, whilst the L_s remains at a similar level. Therefore, the choice of superconducting material used should take into account the operational frequency band of the KITWPA, not simply pursuing high L_s and low R_s film.

Table 1. Critical parameters of various generic BCS (Bardeen–Cooper–Schrieffer) superconducting thin films under investigation, where T_c is the critical transition temperature, V_{gap} the gap voltage, f_{gap} is the gap frequency, f_{frac} is the fractional frequency (f/f_{gap}) and ρ_N is the normal state resistivity. Al, Aluminium; Nb, Niobium; NbN, Niobium Nitride; NbTiN, Niobium Titanium Nitride; Ti, Titanium; TiN, Titanium Nitride.

Film	T_c (K)	V_{gap} (mV)	f_{gap} (GHz)	f_{frac} (at 10 GHz)	ρ_N (μΩcm)	Ref.
Al	1.228	0.37	89	0.11	0.63	47
Nb	9.2	2.8	677	0.014	2.85	48
NbN	14.63	4.44	1,073	0.01	220	49
NbTiN	14	4.25	1,027	0.01	100	7
Ti	0.588	0.17	41	0.24	59	44
TiN	4.39	1.33	321	0.03	140	50

Similarly, Figure 3 shows the behaviour of R_s and L_s with the film thickness at 10 GHz. The references shown in the plot refer to the film thickness reported in the literature that have shown to have successful operation of parametric amplification. Using this information, we have charted out an area of R_s and L_s that has shown to be working well for KITWPA, as the baselines for this study. Note that strictly speaking the R_s curves indicate the upper limit for the thickness used of a certain film, while the L_s curves indicate the lower limit, since as mentioned earlier, films with higher L_s and lower R_s are preferred here.

In the first instance, Figure 3 seems to suggest that only three films fall within the grey area regime i.e., the NbTiN, NbN and TiN. However, as the R_s and L_s is inversely proportional to the film thickness, one notes immediately that in fact the Ti film could also work if the film is much thicker than 220 nm, while the non-conventional Al and Nb would also work albeit with an unreasonably thin film (<2 nm). This finding is interesting, as it indicates that as long as we can control the film thickness, all of these films (or in fact any superconducting films) will be feasible for developing a functional KITWPA. Again, this shows that the intrinsic properties of the film are not as strictly important as one may have thought, as long as other film's properties such as thickness can be adjusted to provide the required L_s and minimal R_s to achieve high gain and low loss parametric amplification process.

Since we assume that a good thin film for a KITWPA would have high L_s and low R_s, it is imperative to find the L_s/R_s ratio for different films. Figure 4 shows this ratio for four thin films under study at 50nm thick at various operating frequencies[1]. The first information gathered from this plot is that the higher

[1]We exclude Al and Nb here because the extremely low L_s value gives rise to an extremely high ratio even with a relatively low R_s value. Also, altering the film thickness would simply shift the entire plot along the vertical axis with higher L_s/R_s ratio for thinner films, as indicated in Figure 3.

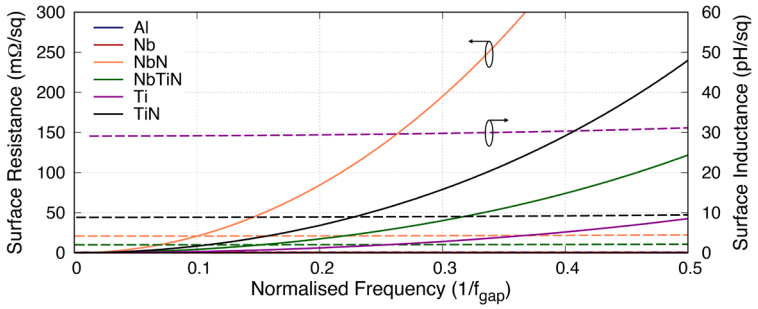

Figure 2. Plot showing the changes in surface impedance with relation to frequency for various 50nm thick BCS (Bardeen–Cooper–Schrieffer) films, where f_{gap} is the gap frequency. Solid lines represent the surface resistance, while the dashed lines represent the surface inductance. It is clear that the surface inductance is only weakly frequency dependent well below the gap frequency, but the surface resistance increases quadratically with frequency. Al, Aluminium; Nb, Niobium; NbN, Niobium Nitride; NbTiN, Niobium Titanium Nitride; Ti, Titanium; TiN, Titanium Nitride.

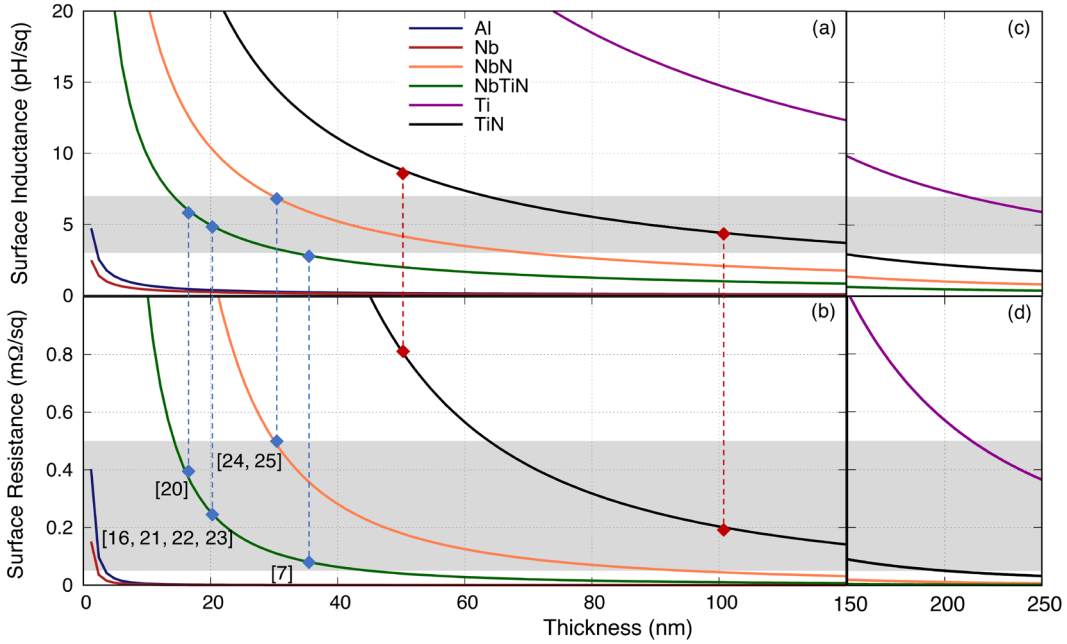

Figure 3. (**a**) Surface resistance and (**b**) inductance of various thin films with different film thickness at 10 GHz, where the dots represent the values reported in the literature. Note that for data point [6] and [7] in the plot, the film used is actually NbTiN but their reported ρ_N and V_{gap} are closer to the value for NbN used in this paper. The two red lines represent the film under consideration for our own works. The grey boxes indicate the range of surface resistances ($0.05< R_s <0.5$ mΩ/□) and inductances ($3< L_s <7$ pH/□) where the KITWPA (Kinetic Inductance Travelling Wave Parametric Amplifiers) samples reported in the literature shows successful operation. (**c**)–(**d**) Extending the film thickness to 250 nm. Al, Aluminium; Nb, Niobium; NbN, Niobium Nitride; NbTiN, Niobium Titanium Nitride; Ti, Titanium; TiN, Titanium Nitride.

the operating frequency, the lower the ratio is, suggesting that for high frequency KITWPA operation one would require high gap superconductor as expected. Secondly, there is no clear trend of the ratio with resistivity ρ_N. Once again, this plot appears to imply that Ti is a relatively good film to use compared to others since it has almost an order of magnitude higher L_s/R_s ratio than other films. However, as noted earlier, this comes with the price of extremely low frequency operation due to the low gap frequency limit. Again, at $f_{op} \rightarrow 10$ GHz, the L_s/R_s ratio for Ti would be at a similar range as NbN. Therefore the use of L_s/R_s ratio to find the optimal film characteristic may leads to unexpected results that is not indicative to the actual performance of the KITWPA.

Although the above plots have provided good information regarding how R_s and L_s change with frequency and film thickness, it is inconclusive which materials or their thickness are optimal for designing a KITWPA i.e., highest L_s with lowest R_s. In Figure 5 we relate the two parameters of interest with the resistivity ρ_N and the gap voltage V_{gap} of various 50nm films. As expected, higher ρ_N would induce higher R_s. However, rather unexpectedly, L_s displays no clear trend with either

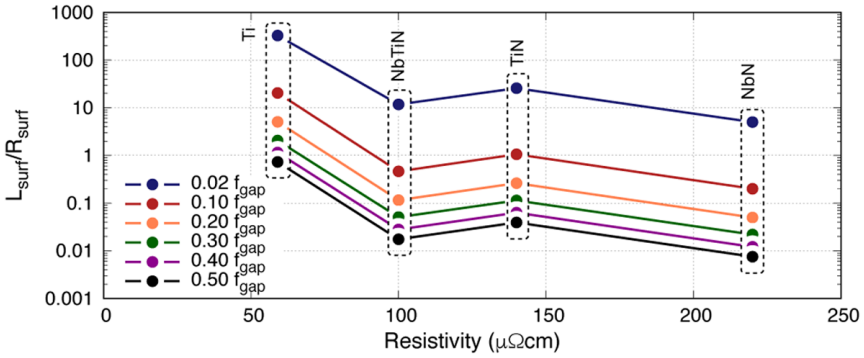

Figure 4. Plot showing the ratio of L_s/R_s (surface inductance/surface resistance) for 50nm thick Ti (Titanium), NbTiN (Niobium Titanium Nitride), TiN (Titanium Nitride) and NbN (Niobium Nitride) at different normalised frequencies, where f_{gap} the gap frequency.

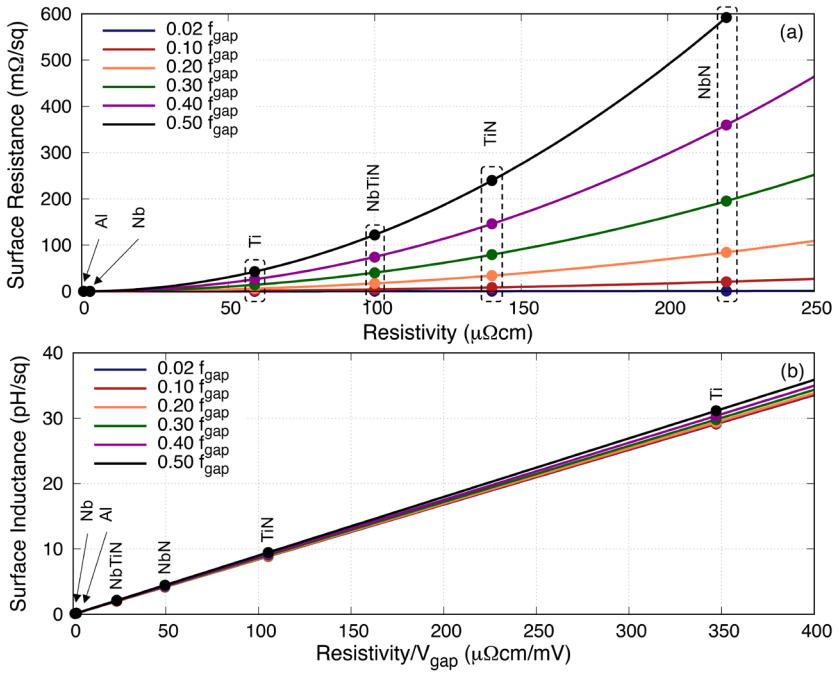

Figure 5. Plots showing the relation between (**a**) surface resistance R_s with resistivity ρ_N and (**b**) surface inductance L_s with the ratio of ρ_N/V_{gap} of various 50nm films at different fractional frequency, where f_{gap} the gap frequency. Ti, Titanium; NbTiN, Niobium Titanium Nitride; NbN, Niobium Nitride; Al, Aluminium; Nb, Niobium; TiN, Titanium Nitride.

ρ_N or V_{gap}, but in fact is linearly proportional to the ratio of ρ_N/V_{gap}. Furthermore, R_s increases significantly with frequency but L_s stays rather constant, just as indicated earlier. These two plots imply that one could in fact control the surface inductance and resistance of the film independently by engineering the film's resistivity and gap voltage. For example, to achieve lower R_s one could lower ρ_N, and in order to retain the same L_s value, we reduce V_{gap} to compensate for the decrease of L_s due to lower ρ_N. This is doable since V_{gap} is not a function of film thickness, therefore we can alter the thickness R_s, once we have engineered the film to have a lower V_{gap}. This solution should be tangible for higher gap superconductor such as TiN, NbTiN and NbN where the operational frequency is well below the gap frequency.

3.1 Engineered TiN thin films

In order to test the above postulate, we have fabricated several batches of TiN films with different Nitrogen flow rates to alter the gap voltage (hence the gap frequency).

We then measured the resistivity of the film[2] to find the relation between V_{gap} and ρ_N. The result is depicted in Figure 6 (a), showing that ρ_N decreases gradually with V_{gap}, but not significantly. In other words, it may seem feasible to

[2]The resistivity was measured at room temperature and corrected by a 1.1 coefficient (obtained from previous experiments) to find the resistivity at cryogenic temperature before the transition temperature.

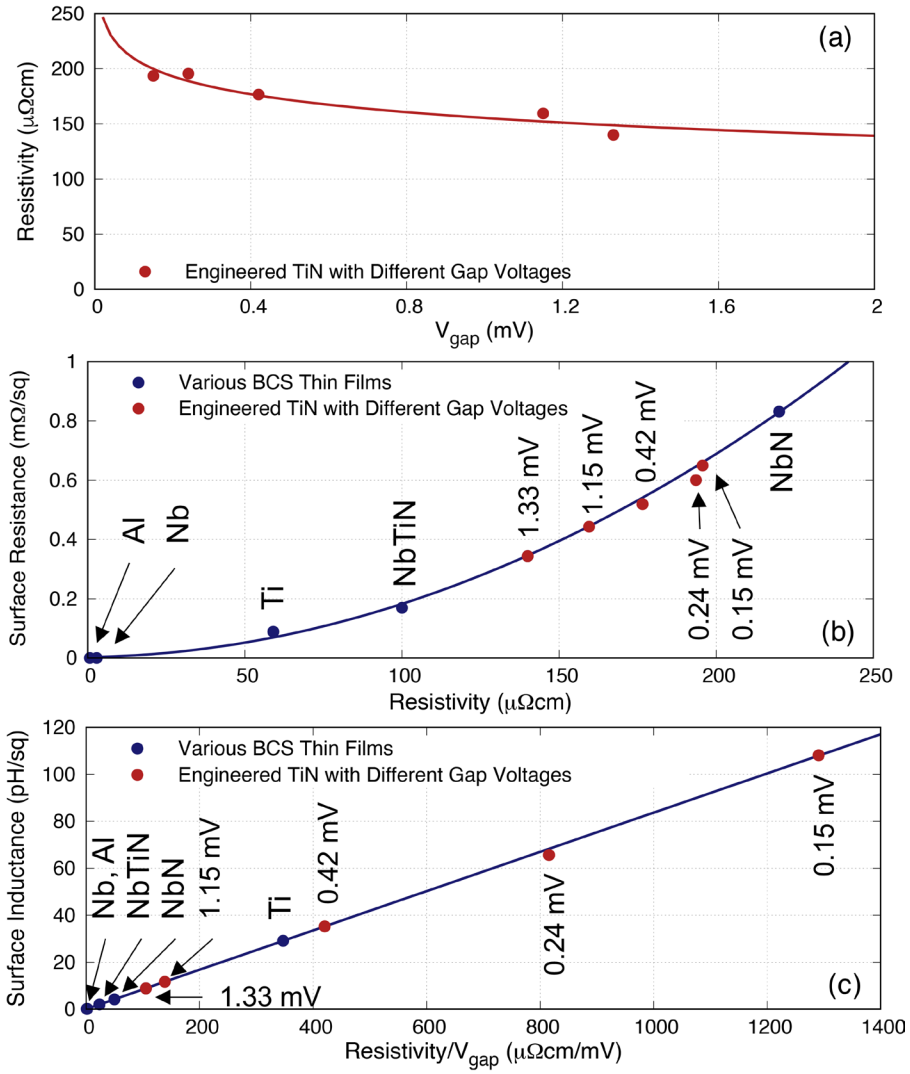

Figure 6. (**a**) Plot showing the resistivity of various engineered TiN film with different gap voltages, where V_{gap} is the gap voltage. (**b**) Relation between surface resistance and resistivity at 0.02 f_{gap} for various BCS (Bardeen–Cooper–Schrieffer) thin films under study, along with the engineered TiN films, all at 50nm thickness. & (**c**) Similar to (**b**) for the relation between surface inductance and the ratio of ρ_N/V_{gap}. The various engineered TiN films are labelled with their corresponding V_{gap}. Ti, Titanium; NbTiN, Niobium Titanium Nitride; NbN, Niobium Nitride; Al, Aluminium; Nb, Niobium; TiN, Titanium Nitride.

assume that ρ_N stays rather constant with large changes in V_{gap} e.g., ρ_N drops only by about 1/3 of its value when V_{gap} is increased from 0.15→1.33mV, almost an order of magnitude higher. This means that although ρ_N will increase slightly (hence higher resistive loss) when V_{gap} is reduced, L_s would increase significantly, hence we can achieve higher L_s while retaining similar level of R_s to produce a KITWPA with much shorter transmission length.

Figure 6 (b) & (c) reproduce the 0.02 f_{gap} curve shown in Figure 5 (a) & (b) but with added points of these engineered TiN films. As can be seen, indeed we can achieve higher L_s with the engineered films, while retaining the R_s within the same range. For example, the TiN film with V_{gap} = 0.42mV is clearly shown to have a lower R_s at 0.52 mΩ/□ but L_s is now much higher, close to 35 pH/□, compared to NbN with R_s = 0.83 kΩ/□ and L_s = 4.2 pH/□. This suggests that our earlier proposed solution may work to achieve higher L_s and lower R_s by engineering ρ_N and V_{gap} of the film.

However, it is obvious that lowering V_{gap} would affect the frequency range in which the KITWPA can operate, as well as the bath temperature. Therefore, it would be indicative to perform the same analysis at a fixed operational frequency instead

of fractional frequency. Figure 7 shows the relation between R_s and L_s for all the 50nm film under study here, including the engineered TiN films, which surprisingly show a clear quadratic relation between the two parameters, and it is consistence regardless of the film types i.e., independent of ρ_N & V_{gap}. This is in stark contrast with our assessment earlier, as this relation shows that the film properties have no significant effect on altering the R_s-L_s relation. In another words, the ideal films would be located near the bottom right of the graph, but clearly from Figure 7 this would be impossible. The reason behind this is because lowering V_{gap} inevitably increases the normalised frequency ($1/f_{gap}$), which in turn increases R_s as shown earlier in Figure 2.

Another interesting observation here is that the quadratic nature of the relation also indicates that the surface resistance increases faster than the inductance when $dR_s/dL_s > 1$. This could indicate that for a successful KITWPA operation at 10 GHz, the thin film used should have an $R_s < 23$ kΩ/□ with $L_s > 3$ pH/□ as shown by the arrows in Figure 7. Figure 8 plots the same R_s-L_s relation for all films with different thickness at different operating frequencies, again showing the same quadratic relation between the two parameters regardless of the film thickness and operating frequency as well. Here, we exclude the engineered TiN films as it makes the plot too crowded to view, but all the points would lie exactly on the 10 GHz curve[3]. Obviously for KITWPA the favourable scenario is high L_s with low R_s as previously stated. However, this relation implies that higher L_s would induce higher R_s regardless of the film's properties, hence it is implausible to reduce the R_s without sacrificing for lower L_s value.

As indicated earlier, the surface resistance increases faster than the inductance above $dR_s/dL_s = 1$, and the situation is worse with higher frequency where the rate of increase (i.e., the derivative of the curve) becomes steeper, in contrast to the low frequency operation where the relation is almost linear. This unfortunately suggests that KITWPA may not work well at high frequencies (e.g., at millimetre-wave regime) even with high gap superconductors, which again was actually already hinted at Figure 2. One may argue that for high frequency operation, one could choose the regime with lower inductance where the R_s-L_s relation is more linear. But this may not lift the predicament because the film needs to have a certain lower limit value of L_s as indicated by the grey box. A clear example is shown by the 40 GHz curve where it does not intersect with the grey box at all. However, it is worthwhile noting that these limits are not fundamental limits but simply the indicative reference points from the working devices reported in the literature. In particular, results reported in 25 showed that their KITWPA could work up to 40 GHz with their NbTiN film (which have closer properties to the NbN parameters used here). Therefore, this may imply that one could in fact tolerate higher resistive loss up until 4 kΩ/□ as shown by the down arrow in Figure 8 (b).

It is interesting to note that the relation between R_s and L_s shown in Figure 6 and Figure 8 is universal and independent of the properties of the thin film used. This may seems counterintuitive, but it is not hard to prove mathematically. From Figure 5, it is clear that $L_s \propto \rho_N/V_{gap}$ and $R_s \propto \rho_N^2$. By rearranging these two equations, we arrive at $R_s \propto (hf_{op}\, L_s/Ne)^2$, where $V_{gap} = hf_{gap}/e$, f_{op} is the operational frequency, $N = f_{op}/f_{gap} = V_{op}/V_{gap}$, and e & h the electron charge and Planck constant. Therefore, the relation between the R_s and L_s is in quadratic nature, with $(hf_{op}/Ne)^2$ as the coefficient, as shown in Figure 6 and Figure 8, and that the slope of the curve scales with frequency. Similarly, the surface resistance is also related to the operating frequency in quadratic fashion with $(hL_s/Ne)^2$ as the coefficient, and as shown in Figure 2, where higher L_s (or ρ_N/V_{gap}) incurs higher R_s.

[3]The 10 GHz curve is exactly the same curve as shown in Figure 7

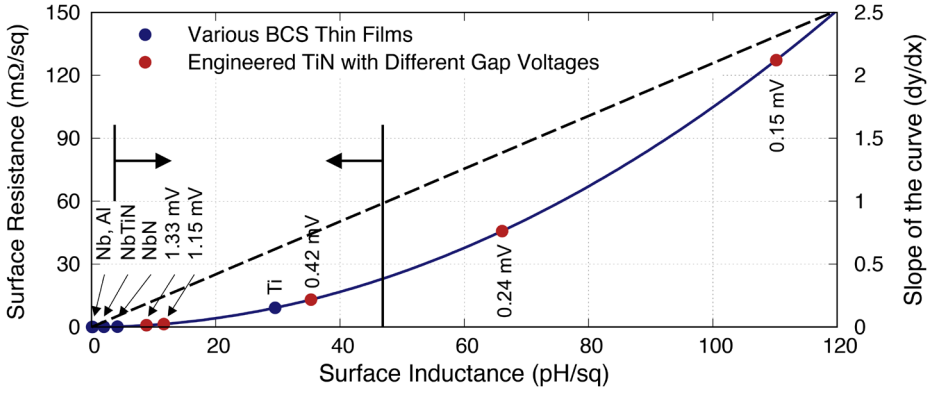

Figure 7. The relation between surface resistance and inductance at 10 GHz for various BCS (Bardeen–Cooper–Schrieffer) thin films under study, along with the engineered TiN films, all at 50nm thickness. The graph shows a clear quadratic relation between R_s (surface resistance) and L_s (surface inductance). The dashed line plots the derivative of the quadratic relation, where the arrows show the possible operational range for KITWPA (Kinetic Inductance Travelling Wave Parametric Amplifier). The lower limit was taken from Figure 3 where $L_s = 3$ pH/□, while the upper limit indicates the point where the slope of the quadratic curve is less than 1. Al, Aluminium; Nb, Niobium; NbN, Niobium Nitride; NbTiN, Niobium Titanium Nitride; Ti, Titanium; TiN, Titanium Nitride.

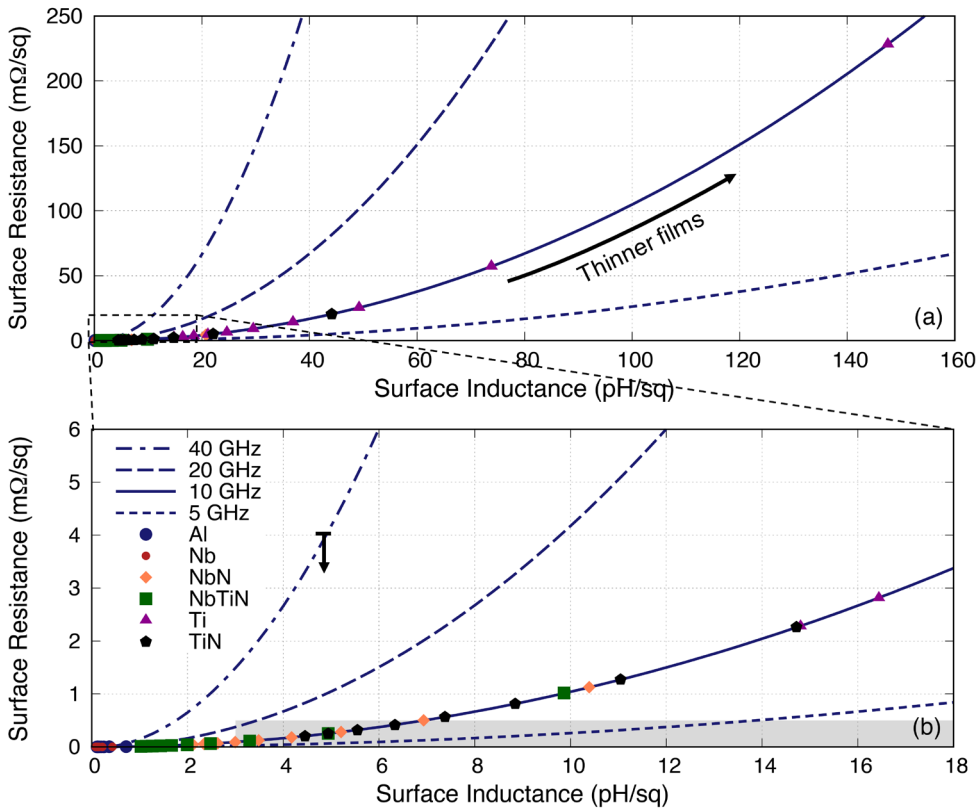

Figure 8. Plot showing the clear quadratic relation between surface inductance and surface resistance of different films with different thicknesses at different operating frequencies (data for TiN shown here refers to the TiN with V_{gap} = 1.33 mV). The surface impedances were calculated from 10nm up to 100nm with 10nm interval shown in dots. The grey box indicates the lower limit of the surface inductance required with the upper limit dictated by the surface resistance before the film gets too lossy (reference to the grey boxed in Figure 3). The thin films that fall in to the greyed out regime is NbTiN with $t \approx 15$–35 nm, NbN with $t \approx 30$–70 nm, TiN with $t \approx 65$–150 nm & Ti with $t > 220$ nm. Al, Aluminium; Nb, Niobium; NbN, Niobium Nitride; NbTiN, Niobium Titanium Nitride; Ti, Titanium; TiN, Titanium Nitride.

These findings are in disagreement to conventional presumption that film with high resistivity or V_{gap} is required for KITWPA operation. In fact, it indicates any superconducting thin films could work as long as the correct thickness is used (below the penetration depth but not too thin to incur too high resistive loss), and that even film such as superconducting Aluminium or Niobium could be used to fabricate KITWPA, albeit with unreasonably thin films.

Therefore, we identify that for our design, we shall focus on the use of 100nm TiN film with V_{gap} = 1.33mV (T_c = 4.39 K) as it has similar R_s and L_s values as most of the successful examples shown in Figure 3. For the following analyses, we further include another option with half the TiN film thickness to show the impact of higher R_s and L_s on the performance of the KITWPA.

4 Substrate and topology considerations

The choice of the superconducting thin film forms only part of the design consideration for developing an optimal KITWPA. The planar circuit amplifier can in principle be formed using any type of transmission line topology fabricated on different varieties of supporting substrate. In this section, we explore how these transmission line topology and substrate choices would affect the performance of the KITWPA. For this exercise, we too make use of *em* simulators Ansys HFSS and the Mattis-Bardeen equations. The source code for calculating the superconducting surface impedance via the Mattis-Bardeen equation, namely the SuperMix software libraries, were previously developed by several contributors at the California Institute of Technology (CalTech), and not by the authors of this article. Source code of SuperMix is available at: here In particular, we focus on the conduction and dielectric losses, the compactness of the device and the feasibility of fabrication in terms of circuit dimensions. Figure 9 shows the four different types of STL topologies we investigate here i.e., coplanar waveguide (CPW), inverted CPW, microstrip, and inverted microstrip line.

Among the chosen four topologies, the inverted lines have the advantage of protecting the long transmission line via the top ground layer, especially the central conductor or the wiring layer, from potential physical damage during handling

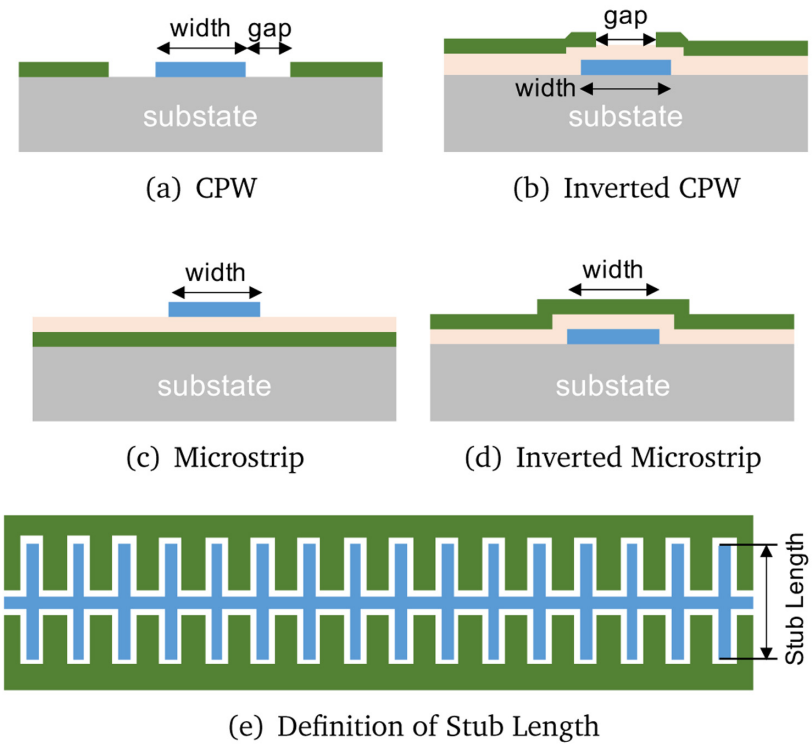

Figure 9. Various types of transmission lines under investigation, where CPW stands for coplanar waveguide. The ground layers are coloured green, dielectric layer light orange and the wiring layer blue. For all the analysis presented, we assume a substrate thickness of 500 μm for all topologies and substrate choice.

of the device such as subsequent chip dicing and wire bonding process after fabrication. This also helps to avoid potential unwanted scratches, which could cause open circuit or debris of conducting materials that cause short circuit to ground. However, the downside of such protective layer is the need for a dielectric layer, which means that the wiring layer is now sandwiched between two non-conductive layers i.e., the thin dielectric layer and the supporting substrate, hence could potentially increase the dielectric losses and induce higher noise due to the two level system (TLS) noise mechanism. On the other hand, conventional CPW and microstrip only have a single contact interface between the wiring layer and the dielectric or the substrate, but it may be prone to mechanical damage as the transmission line is now completely exposed.

As we have shown that the choice of superconducting thin film is relatively unimportant as long as the thickness of the film can be controlled accurately, for all the following analysis, we shall only focus on the TiN film with a T_c = 4.39 K. We include both 50nm and 100nm options to demonstrate the effect of the relative surface resistance and inductance. For all the STL topologies under study here, we assume that the dielectric layer is formed using silicon monoxide (SiO) with a resistivity $\rho = \infty$, dielectric loss tangent tan δ = 0.004 and relative permittivity ε_r =5.8. We explore three different types of commonly used substrate i.e., high resistivity silicon, sapphire and quartz (the characteristics of these substrates are listed in the footnote of Table 2), all with the same thickness of 500 μm. All the transmission line dimensions are optimised to achieve a characteristic impedance Z_0 of 50Ω to match the impedance of the external circuitry. Due to this requirement, we exclude the choice of generic CPW because the typical dimensions used for this type of STL would result in a much higher Z_0 because of the high surface kinetic inductance ($Z_0 \propto \sqrt{L/C}$) of the film[4]. Instead, we relax the need for an unrealistically small gap (increase C) or large central strip width (to reduce the geometric L), by introducing a series of capacitive stubs along the CPW as shown in Figure 9 (e) to significantly increase the shunt capacitance while retaining a similar value of surface inductance[22,33].

From Table 2 and Table 3, one immediately notes that the transmission (insertion) loss of the CPW in terms of S_{21} is much

[4]Even with 100nm TiN that posses lower surface resistance, the central strip to gap width aspect ratio is still formidably high, closed to 10:1 for sapphire and silicon, and 60:1 for quartz, which is not realistic and it may excite unwanted modes even with equipotential bridges. The scenario is even worse with thinner film that have higher inductance.

Table 2. Electromagnetic characteristics of different types of transmission lines on different substrates for a 50nm thick TiN with T_c = 4.39 K. Here we assume an SiO (silicon monoxide) thickness of 100 nm. CPW, coplanar waveguide; TiN, Titanium Nitride.

	Silicon[1]			
	CPW	**Inv. CPW**	**Microstrip**	**Inv. M-strip**
Width	10 µm	5 µm	2.1 µm	2.0 µm
Gap	5 µm	4.65 µm	NA	NA
L_{stub}	72 µm	NA	NA	NA
$L_{\lambda/2}$[5]	910 µm (30 stubs)	750 µm	350 µm	330 µm
S_{21}:10 GHz[4]	–1.10 dB	–2.88 dB	–3.87 dB	–3.59 dB
S_{21}:30 GHz[4]	–4.27 dB	–12.89 dB	–16.84 dB	–15.81 dB
	Sapphire[2]			
	CPW	**Inv. CPW**	**Microstrip**	**Inv. M-strip**
Width	10 µm	5.05 µm	2.1 µm	1.95 µm
Gap	5 µm	4.65 µm	NA	NA
L_{stub}	101 µm	NA	NA	NA
$L_{\lambda/2}$	830 µm (28 stubs)	785 µm	340 µm	336 µm
S_{21}:10 GHz	–0.37 dB	–2.66 dB	–4.15 dB	–3.75 dB
S_{21}:30 GHz	–3.33 dB	–12.61 dB	–17.90 dB	–16.72 dB
	Quartz[3]			
	CPW	**Inv. CPW**	**Microstrip**	**Inv. M-strip**
Width	10 µm	5.24 µm	2.1 µm	2.03 µm
Gap	5 µm	4.65 µm	NA	NA
L_{stub}	288 µm	NA	NA	NA
$L_{\lambda/2}$	725 µm (24 stubs)	785 µm	350 µm	345 µm
S_{21}:10 GHz	–0.31 dB	–3.36 dB	–3.87 dB	–3.92 dB
S_{21}:30 GHz	–3.05 dB	–14.88 dB	–16.84 dB	–17.17 dB

[1]Relative dielectric constant ϵ_r =11.9, resistivity ρ =15 kΩcm, loss tangent tan δ=1.2×10^{-5}.

[2]ϵ_r =9.4, ρ =∞, tan δ=8.0×10^{-8}.

[3]ϵ_r =3.78, ρ =∞, tan δ=0.

[4]70 wavelengths at 24 GHz.

[5]At 24 GHz.

[6]L_{stub} is the length of the stubs, $L_{\lambda/2}$ is the half wavelength length of the section at 24 GHz and S_{21} is the insertion loss.

Table 3. Electromagnetic characteristics of different types of transmission lines on different substrates for a 100nm thick TiN with T_c = 4.39 K. The SiO (silicon monoxide) thickness is increased to 200nm for easier match to Z_0 = 50Ω to avoid need for narrow strip line. The symbols used in the table are given in Table 2. CPW, coplanar waveguide; TiN, Titanium Nitride.

	Silicon			
	CPW	**Inv. CPW**	**Microstrip**	**Inv. M-strip**
Width	10 µm	5.06 µm	2.16 µm	1.93 µm
Gap	5 µm	5 µm	NA	NA
L_{stub}	50 µm	NA	NA	NA
$L_{\lambda/2}$	1.27mm (42 stubs)	1.19mm	650 µm	600 µm
S_{21}:10 GHz	–0.91 dB	–2.00 dB	–3.47 dB	–3.07 dB
S_{21}:30 GHz	–2.17 dB	–7.36 dB	–13.03 dB	–11.58 dB
	Sapphire			
	CPW	**Inv. CPW**	**Microstrip**	**Inv. M-strip**
Width	10 µm	5.18 µm	2.16 µm	2 µm
Gap	5 µm	5 µm	NA	NA
L_{stub}	74 µm	NA	NA	NA
$L_{\lambda/2}$	1.14mm (38 stubs)	1.2mm	650 µm	610 µm
S_{21}:10 GHz	–0.14 dB	–1.87 dB	–3.47 dB	–3.04 dB
S_{21}:30 GHz	–1.26 dB	–7.66 dB	–13.03 dB	–11.79 dB
	Quartz			
	CPW	**Inv. CPW**	**Microstrip**	**Inv. M-strip**
Width	10 µm	5.48 µm	2.16 µm	2.1 µm
Gap	5 µm	5 µm	NA	NA
L_{stub}	235 µm	NA	NA	NA
$L_{\lambda/2}$	840 µm (28 stubs)	1.25mm	650 µm	625 µm
S_{21}:10 GHz	–0.10 dB	–2.55 dB	–3.42 dB	–3.21 dB
S_{21}:30 GHz	–0.98 dB	–9.71 dB	–12.87 dB	–12.20 dB

lower than the other three STLs. This is because the effective dielectric loss seen by the CPW electric field lines is in fact half of that the substrate dielectric constant, as the top half of the field is above the CPW and travels in the free space. In other words, the filling factor is 50% because the field lines are evenly divided between the free space and the substrate; whereas the inverted CPW has a majority of the fields enclosed between the top ground plane and the substrate. For microstrips and inverted microstrips, the field lines are tightly confined within the thin dielectric layer, hence the losses are inevitably higher.

However, microstrip and inverted microstrip line have the benefit of shorter physical length (due to higher geometrical

shunt capacitance), and hence can produce a much compact KITWPA design and potentially increase yields due to a smaller footprint area for damage. The microstrip family is also easier to design, as CPW tents to generate higher unwanted modes if not being designed properly. Therefore, for the CPW families simulated here, equipotential bridges are deployed along the line to ensure that the two ground planes are consistently in electrical contact. From the point of view of insertion loss, it is easy to conclude that inverted CPW offers no advantage compared to the other STLs as it is as lossy as the microstrip family, but have comparative long electrical length like the CPW. Comparing the microstrip with the inverted microstrip, it can be easily noted that the performances are relatively similar, but the inverted microstrip offers additional protective layer in terms of the top ground plane, with the only downside that it may induce higher TLS losses.

In terms of the substrate choices, one notes immediately from Table 2 and Table 3 that the characteristics of the microstrip family are relatively unaffected by the choice of the substrate as the field lines are concentrated in the dielectric layer. However, we can see that for case of CPW, silicon generally induces higher loss than sapphire and quartz which are ceramic in nature ($\rho = \infty$), whereas silicon is a semiconductor that can partially conduct current. Hence, even with a very high substrate resistivity of ρ =15 kΩcm, the losses are still visibly higher due to the long transmission length. Between sapphire and quartz, the latter induces the lowest loss because it has the lowest loss tangent, but the length of the capacitive stubs (L_{stub}) increases substantially compared to silicon and sapphire due to the low relative permittivity. The effective wavelength of both ceramic substrates also decreases compared to silicon, hence requiring fewer stubs with shorter physical STL length. Therefore, we conclude that for case of CPW, sapphire is the optimal choice as it's less lossy than silicon and requires significantly shorter stubs than quartz, hence reducing the footprint of the amplifier chip.

Comparing the difference between using 50nm and 100nm TiN film, we note that the S_{21} loss is less with the 100nm film, as the surface resistivity is lower. However, as discussed in the earlier section, lower R_s indicates lower L_s, therefore the effective wavelength is now longer (requiring more stubs). Nevertheless, the stub length is relatively short for the 100nm film, hence compensating for the higher number of stubs required, and most probably would result in a similar compactness in terms of the amplifier footprint. Note that the width of the microstrip line is similar for both 50nm and 100nm cases. In principle this should not be the case since a lower R_s from the 100nm film will decrease Z_0 and hence a narrower line is needed to reduce the shunt capacitance and increase geometric inductance to achieve Z_0 = 50Ω. However in our case, we opt to increase the thickness of the SiO layer from 100 nm to 200 nm, hence effectively reducing the shunt capacitance to avoid the need for much narrower line width that could be difficult to fabricate using standard photolithography techniques, especially to maintain the consistency of width for such a long transmission length. Furthermore, with narrow microstrip, the characteristic impedance becomes more sensitive to the width and hence more susceptible to the fabrication error, affecting our ability to achieve 50Ω line accurately.

In summary, the use of a thinner 50nm film results in higher losses compared to the 100nm film but requires shorter transmission length. A CPW has the lowest insertion loss among all STL topologies, especially with sapphire or quartz substrate, but the stub length for using quartz become inconveniently long, hence the use of sapphire substrate is a better option. An inverted CPW may produce more compact amplifier design as it can achieve 50Ω characteristic impedance without the need for capacitive stubs, but the loss is high, similar to the level of the microstrip family, hence offers no added advantage here. For the microstrip and the inverted microstrip, their characteristics are largely similar, and are unaffected by the choice of substrate. However inverted microstrip allows for protection of the main transmission line from potential physical damage, as well as better thermalisation as the wiring layer is now directly in contact with the substrate. Therefore, we identify that to achieve the lowest loss (hence least resistive heating) design with relatively small footprint, one should opt for using the 100nm film forming a CPW with capacitive stubs on top of sapphire. On the other hand, to achieve a more compact KITWPA design with shortest effective wavelength, we should choose inverted microstrip design with 50nm thick TiN. We shall include both designs in the subsequent sections and compare their characteristics and performances.

5 Designs of KITWPA

In this section, we perform the gain-bandwidth product prediction using the method presented in Section 2 for both KITWPAs identified earlier. Please note that all data underlying the graphs and the scripts for plotting the graphs are available in *Underlying data* and *Extended data*[51]. To achieve exponential gain, the power dependent phase difference between all the propagating tones needs to be minimised. As explained previously, this can be done by altering the dispersion relation of the transmission line through periodically varying the impedance along the line i.e., the periodic loading scheme. Here, we aim to achieve more than 20 dB gain centred at 8 GHz with minimal length for compactness. For an optimal amplifier design, we take into account considerations that are needed to mitigate risk of physical damage, promoting uniformity of the transmission line, and target for minimum pump power requirement. The last requirement is important as the coupled mode equations assume $I_p \ll I_0$, hence at high pump power level, the gain-bandwidth prediction may not be completely reliable anymore. Furthermore, high pump power could also potentially increase amplifier noise through the resistive loss.

As explained in Section 2, for these simulations, we include all the loss mechanisms such as substrate resistivity, dielectric loss tangent etc., as well as the equipotential bridges for the case of CPW amplifiers, as the added extra capacitance from these bridges would slightly shift the propagation length as well as reducing the radiative loss.

5.1 Validation of design methodology

Before we start to simulate the KITWPA using the methodology presented in Section 2, to ensure that the proposed method is feasible, here we reproduce the gain-bandwidth product of a measured KITWPA reported by Chaudhuri *et al.*[22] using the information provided in the paper. The KITWPA

was designed to operate at a central frequency of ~6 GHz and was fabricated using 20nm niobium titanium nitride (NbTiN, T_c = 15 K) film deposited on top a silicon substrate. The transmission line is configured as a coplanar waveguide (CPW) with capacitive stubs as shown in Figure 10(a) to achieve a 50Ω line. The central strip and gap width of the CPW and the stubs are 2 μm wide, and the capacitive stub length is reduced by a factor of 5 at every one-sixth of a wavelength (λ_0) at the central frequency (increasing the characteristic impedance from 50 to 111Ω) to create the stopbands at ~18 GHz for pump's third harmonic suppression. The length of every third loading sections is doubled from 2 to 4 stubs to create the sub-stopbands at 6 and 12 GHz. Here, the unit cell is formed by interweaving three 50Ω sections with three loading sections, and the total electrical length of the amplifier is 140 unit cells long.

Using the method described above, we calculate the parametric gain of the KITWPA. As shown in Figure 10(b), we could reproduce the 9 dB gain of the KITWPA as claimed in 22. In the paper, they reported that they cascaded two of these linear amplifiers to achieve greater than 15 dB gain. Therefore, we further simulated the gain of the cascaded KITWPAs by taking the output signal amplitude of the first amplifier as the input to the second KITWPA. As shown in Figure 10(b), we managed to obtain the gain curve that is very close resemblance to the measured performance shown in Figure 3 of 22. Therefore, we are confident that our proposed method can accurately predicts the gain-bandwidth performance of a KITWPA.

5.2 CPW with 100nm TiN film

In this section, we focus on the design of the CPW parametric amplifier that is topologically similar to the example shown above but formed using 100nm TiN film on a sapphire substrate. Here we utilise a similar periodic loading scheme for phase matching and pump's third harmonic suppression, except we alter the characteristic impedance Z_0 of the third loading section by removing the capacitive stubs (instead of the loading length) to increase the difference between the third loading impedence to the primary loading impedance, and thereby produce stronger sub-stopbands for dispersion correction. The dimensions of the 50Ω main transmission line, the primary loading section and the third loading section making up the unit cell is tabulated in Table 4.

As we mentioned earlier, it is imperative to ensure that the pump power is minimised while achieving the targeted gain, as a higher pump current would induce higher resistive loss and the coupled mode equations cannot accurately predict the performance of the KITWPA at high pumping levels. Therefore, we first investigate the relation of the pump power with the parametric gain for different number of total unit cells i.e., the total length of the amplifier, as shown in Figure 11(a). One striking observation here is that the gain does not pick off before $I_p \approx 0.3I_0$ for all cases with different length of KITWPA, cascading from 50 to 150 unit cells, and the slope of the gain curves becomes steeper with longer transmission length i.e., the more unit cells there is, the faster the amplifier can reach maximum gain at lower pump power. However, the onset where the signal tone starts to experience gain does not occur until higher pump current values compared to the shorter amplifier option. This behaviour is consistent with the phase mismatch relation to the gain as explained in Section 2, and illustrated in Figure 11(b). One noted that the total phase mismatch Δ_ϕ at low I_p for longer transmission length is further away from the zero axis compared to the shorter option, hence the onset at higher pump amplitude, even though the rate of approaching $\Delta_\phi = 0$ axis is faster for longer length. These plots are important as it shows that to achieve moderate gain of 20 dB, it may not be necessary to opt for longer transmission line. As shown in Figure 11(a), once the amplifier is 100 unit cells long, we can achieve 20 dB gain at around $I_p \approx 0.4I_0$, similar to 125 and 150 unit cells options. Since shorter transmission length will reduce risk of physical

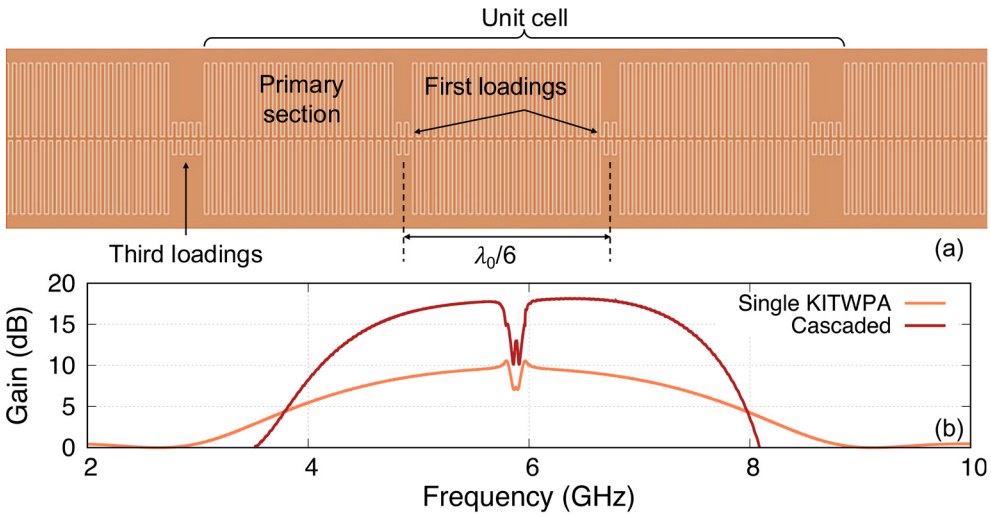

Figure 10. (**a**) Topology of a KITWPA (Kinetic Inductance Travelling Wave Parametric Amplifier) reported in 22, where λ_0 is the central frequency wavelength. (**b**) Simulated gain-bandwidth profiles of the amplifier using the method presented in this paper.

damage and results in smaller foot print, we therefore concluded that the optimal design in this case would be a KITWPA with 100 repeated cells.

Table 4. Dimension of the transmission line forming a single unit cell for the CPW (coplanar waveguide) KITWPA (Kinetic Inductance Travelling Wave Parametric Amplifier) on a sapphire substrate, where Z_0 is the characteristic impedance and L_{stub} is the length of the stubs.
TiN, Titanium Nitride.

	CPW with 100nm TiN film		
	Primary Line	**1st Loading**	**3rd Loading**
Z_0	50Ω	60Ω	90Ω
Width	10 μm	10 μm	5.7 μm
Gap	5 μm	5 μm	5 μm
L_{stub}	74 μm	36 μm	NA
Length	34 stubs	4 stubs	200 μm

One would expect that the parametric gain would increase exponentially with I_p at all values, but as shown in Figure 11(a) this is not the case. The maximum gain plateaus at around 55 dB. This is because the signal amplitude at this pump current level is now higher than the pump current itself, hence the energy starts to flow backward from the signal to the pump. This is shown clearly in Figure 11(c) that depicts the case of a 100 cells amplifier, showing how the pump starts to deplete near $I_p \approx 0.56I_0$ and reach a minimum at $I_p \approx 0.67I_0$ where the signal amplitude peaks. After this point, the signal amplitude starts to deplete and the pump slowly regains its amplitude, hence the oscillating behaviour between the two tones as shown in Figure 11(a). One should note that the position of this peak gain is dependent on the total phase mismatch of the amplifier Δ_ϕ as well, as illustrated in Figure 11(b), because this parameter is dependent on the pump amplitude as well. The maximum peak gain near 55 dB and its location are also dictated by the initial signal amplitude used in the calculation where in our case we assumed $I_s(0) = 10^{-3}I_p$, and with lower $I_s(0)$ the higher the maximum gain would be, and peak at higher I_p, as the signal amplitude requires higher gain to be comparable to the pump amplitude.

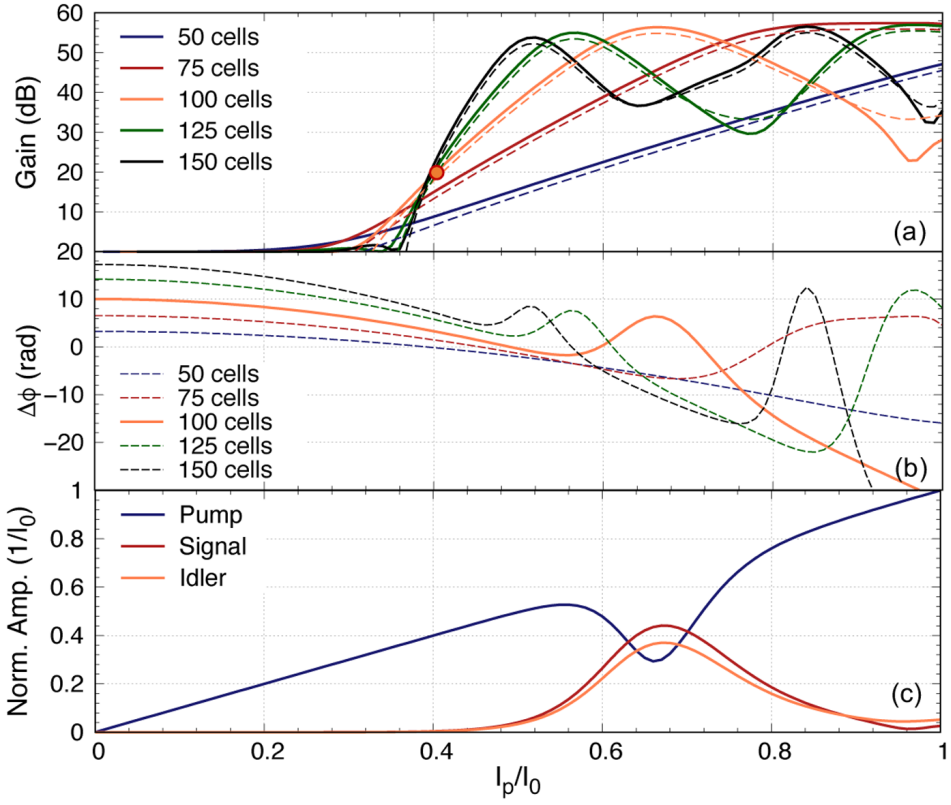

Figure 11. (**a**) The relation of parametric gain plotted against the pump power for different length of the amplifier, where Δ_ϕ is the total phase mismatch and I_0 is the critical current. The solid line represent the signal gain, while the dashed line the idler gain (reference to input signal power). (**b**) The total phase mismatch plotted against the pump power. (**c**) Curves showing the relation between the pump, signal and idler tones reacting to each other for the 100 cells amplifier. All curves were plotted with signal frequency of 9 GHz and pump frequency of 7.649 GHz.

One important observation of Figure 11(b) is that at the point where the peak gain occurs, the phase mismatch $\Delta_\phi \neq 0$. This implies that we may have over compensated the phase correction before the pump starts to deplete as the excursion of the dispersion relation is related to the ratio of the impedance of the third loading section to the primary loading section. Furthermore, we would like to explore if there is a method to further reduce the required pump current. As the dispersion diversion from the otherwise linear dispersion relation is directly related to the ratio of the third loading impedance with the primary loading section, another way to reduce the overcompensation of the dispersion is by reducing this impedance difference. Here we investigate if we can achieve higher gain with lower pump current by using different Z_0 for the third loading. The result is shown in Figure 12, and we include the case of a linear amplifier without any periodic loading, notated as 50Ω curve in the plot. Again, we see that to achieve 20 dB gain, all the plots converge at $I_p = 0.4I_0$. However, from Figure 11 we learn that with longer line, the rate to achieve maximum gain is steeper, hence we can in fact increase the number of unit cells to achieve 20 dB gain with lower I_p, and this is indeed the case (see Figure 12(b) and (c)), but at the expense that we now need close to 250 unit cells to reduce the I_p from 0.4 to 0.25. In short, it is possible to reduce the gain onset point to lower I_p value and hence reduce the required I_p value to achieve 20 dB gain but one would need much longer transmission length.

Another way we can reduce the overcompensation of the phase mismatch is by placing the pump frequency further away from the 8 GHz stopband to reduce the overcorrection and we explore this solution in Figure 13 for the case of 100 unit cells amplifier. The downside of this option is that it may result in a larger zero-gain gap. This differs from previous analysis where we always place the pump at the first peak closest to the stopband as shown in Figure 13(a) because the dispersion excursion is maximised at this point with the lowest insertion loss, here we explore the difference in gain behaviour if we place the pump frequency at subsequent peaks further away from the primary stopband. Note that this is another advantage of using the methodology described in this paper, where we can effectively capture the behaviour of the cascaded cells, which produce the 'ringing' effect near the stopbands, that is not possible with translation symmetry assumption used in most models reported in literature. So here, we investigate the same I_p vs gain relation by placing the pump at different frequencies to try to achieve $\Delta_\phi = 0$ before the pump depletion kicks in. Note that the insert in Figure 13 shows exactly how we suppressed the pump's third harmonics by having a large stopband at $3f_p$.

As we can observe from Figure 13(b) that by choosing different pump frequency, indeed we can achieve the onset point at lower I_p value, but to achieve 20 dB gain, we only reduce I_p by about 5%. It is clear therefore, the optimal case here if we pump the amplifier at the second peak where one note that $\Delta_\phi = 0$ near $I_p = 0.4I_0$ now. The gain at this point starts to drop if we shift further away with higher peak number, as the total phase mismatch once again deviates away from the zero axis. The upside of this is that the second peak is only 0.05 GHz away from the first peak, hence would not widen the zero-gain gap too drastically. This combination is therefore the optimal design we can achieve with the CPW amplifier. In Figure 14, we plot the gain

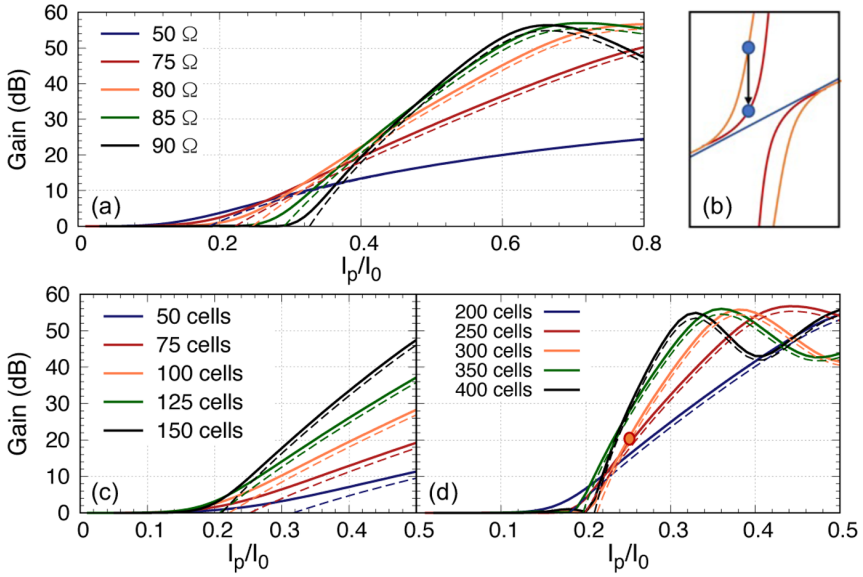

Figure 12. (**a**) The parametric gain plotted against pump power for a 100 unit cells KITWPA (Kinetic Inductance Travelling Wave Parametric Amplifier) with different Z_0 value for the third loading, where I_p and I_0 is the pump current and the critical current respectively. The gain onset starts earlier with lower pump power if the third loading Z_0 is closer to the primary loading impedance. (**b**) Sketch illustrates how the dispersion relation is differ if Z_{03} is decrease from 80Ω (orange) to 75Ω (red), therefore reduces the extra dispersion if the pump frequency remains at the same position. (**c**) & (**d**) Gain versus pump power for different length of KITWPA with Z_{03} = 75Ω. All curves were plotted with signal frequency of 9 GHz and pump frequency of 7.649 GHz.

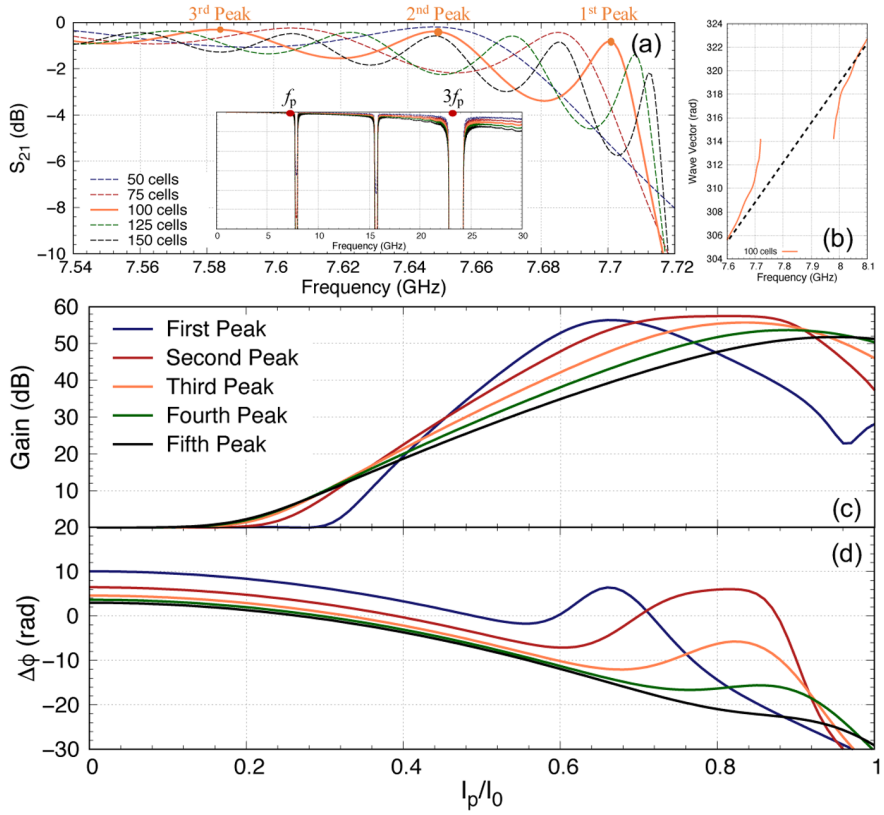

Figure 13. (**a**) The insertion loss of the KITWPAs (Kinetic Inductance Travelling Wave Parametric Amplifiers) with different lengths near the first stopband around 8 GHz, showing the peaks with lowest loss, where I_p and I_0 is the pump current and the critical current respectively and f_p is the pump frequency (**b**) The dispersion relation of the 100 unit cells KITWPA. (**c**) The parametric gain and (**d**) total phase mismatch of the 100 unit cells KITWPA with the pump frequency fixed at different peak positions. All curves were plotted with signal frequency of 9 GHz.

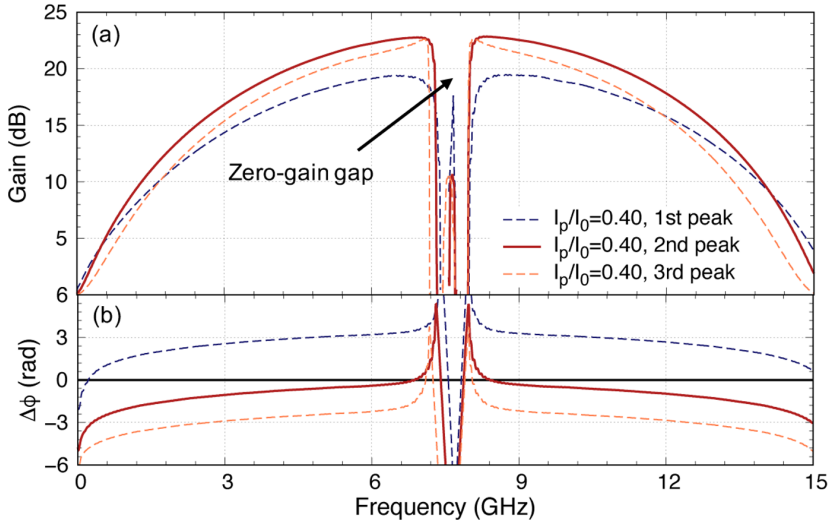

Figure 14. (**a**) The gain-bandwidth profile of a 100 unit cells KITWPA (Kinetic Inductance Travelling Wave Parametric Amplifier) with pump frequency placed at first, second and third peak of the insertion loss curve, where I_p and I_0 is the pump current and the critical current respectively and Δ_ϕ is the total phase mismatch. (**b**) the total phase mismatch corresponding to (**a**). The gain bandwidth is broadest with pump frequency placed at the second peak, where the total phase mismatch is closest to zero over the broadest bandwidth.

profile of this optimal KITWPA with 100 unit cells pumped at $I_p = 0.4I_0$ with the pump frequency located at the second peak, where Δ_ϕ is closest to zero across the broadest bandwidth, hence achieving 20 dB gain with the broadest bandwidth as well.

5.3 Inverted microstrip with 50nm TiN film

Similar to Subsection 5.2, in this section we focus on the design of a compact KITWPA comprising 50nm thin TiN film in the form of inverted microstrip deposited on a sapphire substrate. Here, we further compare the use of different types of dielectric layer for inverted microstrip structure with silicon dioxide (SiO_2) and amorphous silicon (aSi), apart from the use of silicon monoxide (SiO) shown earlier. The properties of these dielectric material, as well as their dimension required to achieve 50Ω characteristic impedance and the transmission loss is tabulated in Table 5. Note that for the case of aSi, with the original thickness of 100nm dielectric layer, we would need a strip width of 1.3 μm to achieve 50Ω ($L_{\lambda/2}$ =255 μm). Therefore we increase the dielectric thickness (t_{diel}) to 200nm such that the width is now closer to 2 μm, to ease the fabrication.

Comparing the three different dielectric materials, one immediately notes that the use of SiO incurs much higher loss than SiO_2 and aSi, due to the high loss tangent of SiO. In principle, aSi should possess less transmission loss compared to SiO_2 as the loss tangent is an order of magnitude lower, but due to the moderately high resistivity, the loss now become comparable to SiO_2. Since the strip width and length is largely similar for all three types of dielectric, we therefore opt for SiO_2 as it has the lowest loss property. Furthermore, fabrication of aSi requires special development procedure and it's not commonly used in the field of microwave cryogenic engineering. It is worthwhile noting that although the effective length of SiO_2 line is slightly longer, it is still shorter compared to the CPW line by close to a factor of three. Without the need for capacitive stubs, we can therefore produce a much more compact amplifier design using this transmission line configuration.

Table 5. Electromagnetic characteristics of 50nm thick TiN (Titanium Nitride) inverted microstrip on sapphire with different dielectric layers, where ϵ_r is the relative dielectric constant, tan δ is the loss tangent, ρ is the resistivity, t_{diel} is the thickness of the dielectric, Ref. is the references, $L_{\lambda/2}$ is the half wavelength length, S_{21} is the insertion loss, SiO is silicon monoxide, SiO2 is silicon dioxide, and aSi is amorphous silicon. The total length used here to calculate the S_{21} is 70 wavelengths at 24 GHz.

	Inverted microstrip		
	SiO	SiO_2	aSi
ϵ_r	5.8	4.0	11.9
tan δ	0.004	3.0×10^{-4}	2.2×10^{-5}
ρ	∞	∞	15 kΩcm
t_{diel}	100nm	100nm	200nm
Ref.	52	53	
Width	1.95 μm	2.40 μm	1.88 μm
$L_{\lambda/2}$	336 μm	400 μm	340 μm

Similar to the CPW KITWPA design, we engineer the dispersion relation of the inverted microstrip KITWPA through the use of periodic loading scheme, where the dimensions and characteristic impedances of each loading sections and the primary 50Ω section are shown in Table 6. Here, we include the analysis for SiO as well as SiO_2 to provide comparison and information with regards to how the loss mechanism may affect the gain-bandwidth product of the KITWPA.

We first investigate the relation between the pump power and the gain of the inverted microstrip KITWPAs with SiO dielectric layer, as shown in Figure 15. One notes immediately that the maximum gain can now only achieve close to 25 dB instead of ~55 dB for the CPW KITWPA with 100nm TiN film, because of the high loss of the inverted microstrip line e.g., with 100 unit cells, we are just about to reach 23 dB gain maximally. Increasing the number of unit cells improves the situation slightly but does not dramatically alter the gain profile. For example, the gain curve for both cases with 125 and 150 unit cells are largely similar, because as the transmission length gets longer, the resistive loss starts to dominate over the parametric gain, hence starts to lower the total gain of the amplifier after 150 unit cells as the pump amplitude is now weaken by the additional loss. From Figure 15(a) and (b), we observed that to achieve 20 dB gain, we would need higher pump power as well, between 40–60% of the I_0 for different number of unit cells. Furthermore, the phase mismatch curves for all 5

Table 6. Dimension of the transmission line forming a single unit cell for the inverted microstrip TWPA (Travelling Wave Parametric Amplifier) on a sapphire substrate with different dielectric layers, where Z_0 is the characteristic impedance, SiO is silicon monoxide and SiO_2 is silicon dioxide.

	SiO		
	Primary Line	1st Loading	3rd Loading
Z_0	50Ω	40Ω	25Ω
Width	1.95 μm	2.60 μm	4.60 μm
Length	336 μm	33.6 μm	33.6 μm
	SiO_2		
	Primary Line	1st Loading	3rd Loading
Z_0	50Ω	40Ω	25Ω
Width	2.40 μm	3.20 μm	5.40 μm
Length	400 μm	40 μm	40 μm

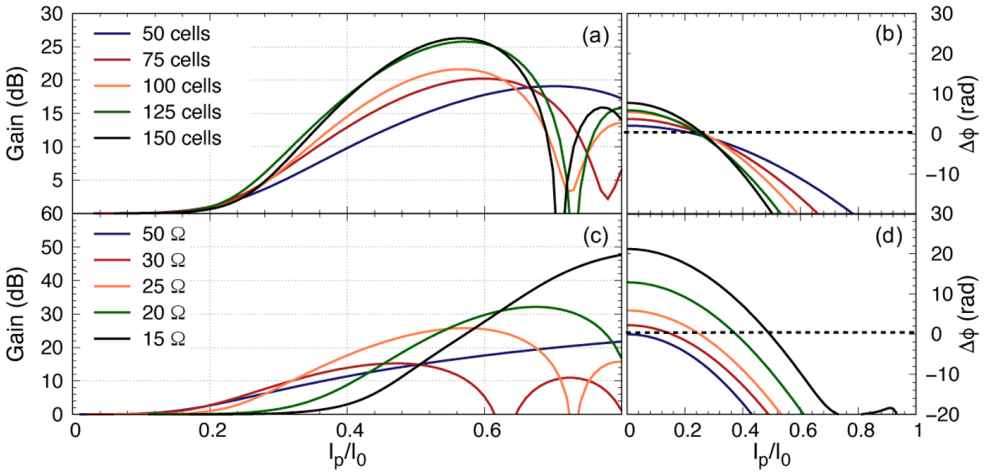

Figure 15. (**a**) The relation of parametric gain and (**b**) phase mismatch plotted against the pump power for different length of the inverted microstrip (Inv. M.S.) KITWPA (Kinetic Inductance Travelling Wave Parametric Amplifier) with silicon monoxide dielectric layer,) with the third loading impedance of 25Ω. (**c**) The parametric gain and (**d**) phase mismatch plotted against pump power for a 125 unit cells KITWPA with different Z_0 value for the third loading. All curves were plotted with signal frequency of 9 GHz and pump frequency of 7.83 GHz.

different lengths cross the zero-axis near $I_p = 0.25I_0$, and diverge from the zero-axis further with longer amplifier length, indicating that we are now under-compensating the phase correction. Both this and the additional loss of the inverted microstrip line contribute to the low gain obtainable by the amplifier despite the use of higher pump power. Therefore, it is important to consider the loss behaviour of the transmission line utilised, because with high loss there may exist an optimal parametric length required, where a shorter line results in low parametric gain, while a longer line incurs high loss which again lowers the overall gain. In the case presented here, it is obvious that we can achieve the best result (highest gain with lowest I_p and shortest length) with 125 unit cells.

As described earlier, we can alter the impedance of the third loading to increase the dispersion divergent to accumulate more phase correction. This approach is shown in Figure 15(c) and (d), where indeed with lower Z_0 (hence larger difference compared to the characteristic impedance of the primary 50Ω line) the Δ_ϕ curves can now reach the zero axis at higher pump level, hence the improvement in the peak gain as well since the parametric gain is improved now. However, the onset of gain now shifted to higher pump amplitude position, hence higher pump current would be needed to achieve the same gain for lower loading impedance, which could be detrimental as explained earlier. Therefore, we conclude that in this particular case, a 125 unit cells KITWPA with third loading impedance of 25Ω is the optimal solution here. This again stressing that in the case of high loss, there indeed exists an optimal solution, where the designer should aim to achieve the desired peak gain that coincides with the maximum gain achievable. In this scenario, the amplitude of the pump is optimum in overcoming the resistive loss and provide high enough power for exciting sufficient parametric gain.

Applying the same analysis and following the similar steps described in Subsection 5.2 including optimising the pump frequency, we shows the predicted gain profiles for both SiO and SiO_2 designs in Figure 16. Both designs utilise a third loading impedance of 25Ω with amplifier length of 125 unit cells for the SiO design and 100 unit cells for the SiO_2 design respectively. The pump current required to achieve the shown gain profile are I_p/I_0=0.50 and 0.38 for SiO and SiO_2 design. As expected, due to the lower loss of the SiO_2 dielectric layer, we can now achieve the similar peak gain with fewer unit cells than the CPW design and lower pump current close to the one utilised for the CPW KITWPA. An interesting feature of these gain profile is that the gain is asymmetric for the SiO design, due to the extremely high loss at the high frequency end, as shown in Figure 16(b). This effectively results in a narrower bandwidth where we can only achieve higher than 20 dB gain from 3.5–10.5 GHz for the SiO design, whilst broader from 3–12 GHz for the SiO_2 amplifier. This exercise once again shows the important of including the loss in the simulation of the KITWPA, as it inevitably has a large effect on the performance of the KITWPA. One important note with regards to the high loss designs is that as the resistive loss is frequency dependent, therefore it would be difficult to operate the KITWPA at higher frequencies, including the option of pumping the amplifier at the second stopband, or operating with the DC-biased 3WM mode, as the pump amplitude would be severely attenuated because the pump is now placed at a higher frequency position. This would mean that most of the pump power is converted into resistive heat loss instead of transferring to the signal wave for amplification.

In Figure 17, we show the actual layout of the two optimised KITWPA designs described in this paper, which have very similar gain-bandwidth product: (a) the low loss CPW KITWPA

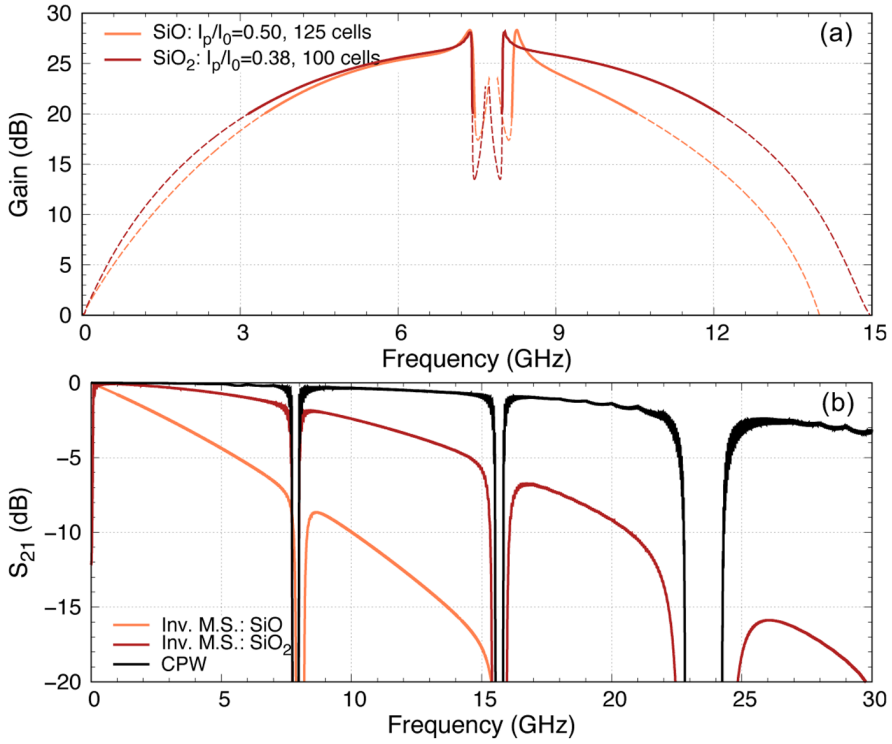

Figure 16. (**a**) Gain profile for the optimised inverted (inv.) microstrip KITWPA (Kinetic Inductance Travelling Wave Parametric Amplifier) with SiO (silicon monoxide) and SiO_2 (silicon dioxide) dielectric layer. (**b**) The S_{21} transmission profile of both inverted microstrip designs compared to the CPW (coplanar waveguide) design presented earlier.

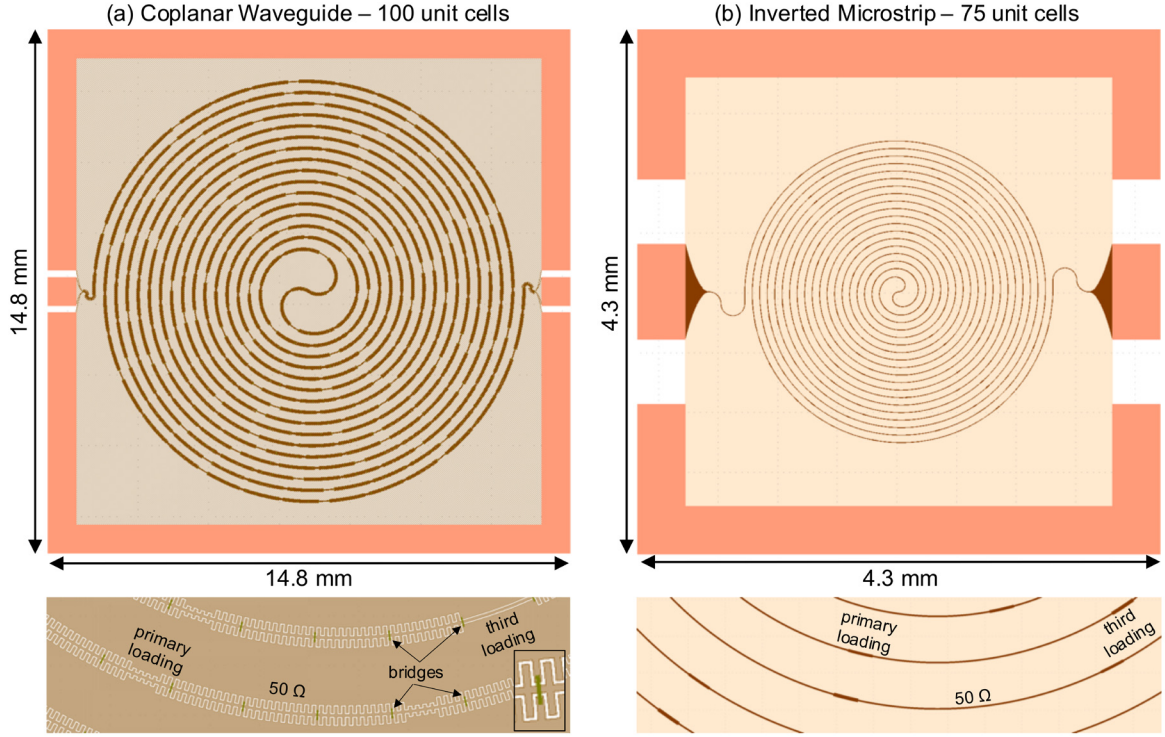

Figure 17. (**a**) The layout of the optimised CPW (coplanar waveguide) KITWPA (Kinetic Inductance Travelling Wave Parametric Amplifier) with 100 repeated unit cells wrapped in a double spiral fashion. The zoomed-in image below shows the various sections making up the unit cells, and a further zoom-in image showing the bridge. (**b**) Similar layout for the optimised inverted microstrip KITWPA.

with 100nm TiN film on sapphire substrate, and (b) the compact inverted microstrip KITWPA with 50nm TiN film with SiO_2 dielectric layer. As mentioned earlier, our simulation for the CPW TWPA includes the existence of the equipotential bridges as shown in the enlarged image of Figure 17, which also illustrate how the primary 50Ω section, the first and third loading section are populated across the entire amplifier. In these particular designs, we opt for winding the long transmission line into a double-spiral form for compactness and low cross talk between the adjacent transmission line. Comparing the two, one immediately notes that the inverted microstrip design is much more compact with a foot print of 3.5×3.5mm compared to the CPW amplifier, which is about 18× smaller in size, dominated mainly by the size of the bonding pads required near the two ends of the amplifier.

Finally, we should emphasise that the reason both KITWPAs design can obtain similar high gain despite the difference in transmission loss is because the higher loss inverted microstrip KITWPA utilises a higher kinetic inductance 50nm TiN film, hence would have higher parametric gain to compensate the additional loss. We demonstrate the effect of properly taking into account the transmission line loss in Figure 18, where we can see that for the lower loss CPW KITWPA, the predicted gain profile is largely similar with or without loss; but for the inverted microstrip KITWPA, if the loss is not included in the calculation, we would over estimate the gain by close to 12 dB. This again shows the important of capturing all the information with regards to the transmission line so that we can accurately predict the performance of the KITWPAs.

Although it may appear that the inverted microstrip design is a better option in this case since it is much compact and less susceptible to physical damage, we should point out that if we take into consideration that with high resistive loss and pump current, the devices may generate more resistive heat as well as additional noise in the form of Johnson noise, then the inverted microstrip design may have inferior noise performance compared to the CPW design. Since most of the energy of the system is carried by the pump wave when the KITWPA is in operation, we can estimate the noise power via $I_{\mathrm{rms}}^2 R$, where the resistance of the wire is given by $\Re(\gamma_p Z_0)$. As our TiN film have a critical current of ~3 mA, and with the corresponding value of I_p/I_0 for each cases, we would arrive at 10.6 μW for inverted microstrip design compared to 1.3 μW for the CPW amplifier, which is almost 10× higher. Hence, there is inevitably a compromise between a small footprint KITWPA and low loss/noise design, and depending on the application, the designer may opt for one over the other based on the preferences.

Nevertheless, our designed KITWPAs are expected to achieve the targeted 20 dB gain, in fact higher gain and hence broader bandwidth with fewer unit cells compared to the results reported in most literatures, demonstrating the feasibility of our method to optimise the performance of a KITWPA. For example, comparing to the design of the KITWPA presented in 22 which only managed to achieve 9 dB gain with 140 unit cells, we manage to reach a peak gain near 25 dB with shorter transmission length around 100 to 125 unit cells. Note that this is close to 30× improvement in amplification of the signal strength with a slightly compact design. Comparing to 7 which operates at the second stopband, again the said amplifier would need 224 unit cells with a pump current much higher than $0.4I_0$ to reach peak gain of 10 dB. Therefore, we trust that we have illustrates that there is indeed room for improvement with the existing design of KITWPA in the literature, and with our approach we could maximise the gain with shortest transmission length and lowest required pump current.

6 Conclusions

In this paper, we have described in detail our procedures and analyses carried out to identify the most suitable superconducting and non-conducting materials required to form a KITWPA, as well as the superconducting transmission line topologies and the operational parameter spaces, to produce a high-gain low loss amplifier that can potentially achieve quantum limited noise performance across broad bandwidth with small foot print. In the first part of the paper, we presented a

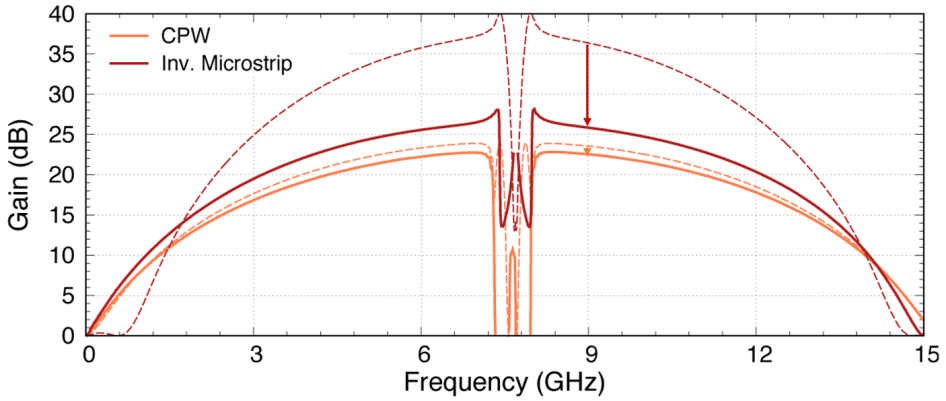

Figure 18. Comparison of gain profile for both CPW (coplanar waveguide) and inverted microstrip KITWPAs (Kinetic Inductance Travelling Wave Parametric Amplifiers) with (solid lines) and without (dashed lines) taking into account the loss in the form of $\alpha_{p,s,i}$. Note that the dashed lines are effectively the actual parametric gains of the device, and with loss the gain would be reduced as expected.

novel method that allows us to fully capture the electromagnetic behaviour of all components making up the amplifier such as the effect of superconductivity, loss tangent, fringing fields etc, and therefore better predict the performance of the KITWPA. This methodology is also very flexible, taking advantages of the versatility of commercial electromagnetic and microwave circuit softwares, and the fast computing coupled-mode equation models, which allows us to explore effect of many different type of materials and transmission line structures that are difficult to simulate using traditional method.

In the second part of the paper, we presented our extensive studies of comparing the performance of KITWPA comprising different type of superconducting materials, in search of a high kinetic inductance and low surface resistance superconducting thin film. We explored their advantages and disadvantages in terms of dependent on operational frequency range, normal resistivity, critical temperature etc, including an engineered TiN film. We found that as long as the thin film behaves in the BCS regime, the choice of the superconducting material has only marginal effect on the performance of the KITWPA. The required kinetic inductance and low surface resistance of any film can in fact be obtained by choosing the appropriate film thickness, as long as it is feasible to fabricate using modern photo-lithography and/or e-beam techniques.

Next, we investigate the most suitable transmission line topology to provide the lowest insertion loss, shortest transmission length and the ease of fabrication (sensible circuit dimensions) to form a TiN KITWPA. We have realised that there is a compromise between achieving low transmission loss with the compactness of the device. A CPW amplifier with thicker film can indeed achieve low insertion loss, but in order to minimise cross talk and the need for capacitive stubs to reach 50Ω characteristic impedance inevitably hinders the compact packing of the transmission line. An inverted microstrip with thinner film, on the other hand, can produce a much shorter effective transmission length than the CPW option, but the higher resistive loss could potentially result in unwanted higher noise performance.

Finally, we report on the design of the two KITWPAs described above, in terms of optimal length required to achieve higher than 20 dB gain with minimal pump power, including the proper placement of the pump frequency and optimising the configuration of the periodic loading scheme to reach exponential gain. In that section, we further illustrated that once the design is optimised, it is possible to operate the KITWPA in different modes, such as operating at higher frequency range, cover broader bandwidth with DC-biasing the device and the potential use of the amplifier in the non-linear regime for high dynamic range applications. We conclude the paper by presenting and comparing the performance of the two optimal KITWPAs including their actual layout and their gain-bandwidth product respectively, for the CPW and the inverted microstrip amplifier, which we pay special attention to the effect of transmission loss on the gain profile of our parametric amplifiers. For both designs, we successfully achieved a predicted gain that is higher than 20 dB with close to 100% bandwidth product with small device area and lower pump current, compared to the existing designs reported in the literature, hence verify the feasibility of our optimised approach for designing a KITWPA.

Data availability

Underlying data

Figshare: Engineering the Thin Film Characteristics for Optimal Performance of Superconducting Kinetic Inductance Amplifiers using a Rigorous Modelling Technique.

https://doi.org/10.6084/m9.figshare.c.6034133.v1[51].

This project contains the following underlying data, organised by ‘dataset’ within the Figshare collection:

- Dataset for Figure 2 (Raw datasets in .dat for each panel in Figure 2)
- Dataset for Figure 3 (Raw datasets in .txt for each panel in Figure 3)
- Dataset for Figure 4 (Raw datasets in .txt for each panel in Figure 4)
- Dataset for Figure 5 (Raw datasets in .txt for each panel in Figure 5)
- Dataset for Figure 6 (Raw datasets in .txt for each panel in Figure 6)
- Dataset for Figure 7 (Raw datasets in .txt for each panel in Figure 7)
- Dataset for Figure 8 (Raw datasets in .txt for each panel in Figure 8)
- Dataset for Figure 10 (Raw datasets in .dat for each panel in Figure 10)
- Dataset for Figure 11 (Raw datasets in .dat for each panel in Figure 11)
- Dataset for Figure 12 (Raw datasets in .dat for each panel in Figure 12)
- Dataset for Figure 13 (Raw datasets in .dat and .csv for each panel in Figure 13)
- Dataset for Figure 14 (Raw datasets in .dat for each panel in Figure 14)
- Dataset for Figure 15 (Raw datasets in .dat for each panel in Figure 15)
- Dataset for Figure 16 (Raw datasets in .dat for each panel in Figure 16)
- Dataset for Figure 17 (Raw datasets in .txt and .csv for each panel in Figure 17)
- Dataset for Figure 19 (Raw datasets in .dat and .txt for each panel in Figure 19)

Extended data

Figshare: Engineering the Thin Film Characteristics for Optimal Performance of Superconducting Kinetic Inductance Amplifiers using a Rigorous Modelling Technique. https://doi.org/10.6084/m9.figshare.c.6034133. v1[51].

This project contains the following extended data, organised by 'dataset' within the Figshare collection:

- Plotting script for Figure 2 (Gnuplot script in .gnu that reads & processes the raw data and plots each panel in Figure 2)
- Plotting scripts for Figure 3 (Gnuplot scripts in .gnu that read & process the raw data and plot each panel in Figure 3)
- Plotting script for Figure 4 (Gnuplot script in .gnu that reads & processes the raw data and plots each panel in Figure 4)
- Plotting scripts for Figure 5 (Gnuplot scripts in .gnu that read & process the raw data and plot each panel in Figure 5)
- Plotting scripts for Figure 6 (Gnuplot scripts in .gnu that read & process the raw data and plot each panel in Figure 6)
- Plotting script for Figure 7 (Gnuplot script in .gnu that reads & processes the raw data and plots each panel in Figure 7)
- Plotting scripts for Figure 8 (Gnuplot scripts in .gnu that read & process the raw data and plot each panel in Figure 8)
- Plotting script for Figure 10 (Gnuplot script in .gnu that reads & processes the raw data and plots each panel in Figure 10)
- Plotting scripts for Figure 11 (Gnuplot scripts in .gnu that read & process the raw data and plot each panel in Figure 11)
- Plotting scripts for Figure 12 (Gnuplot scripts in .gnu that read & process the raw data and plot each panel in Figure 12)
- Plotting scripts for Figure 13 (Gnuplot scripts in .gnu that read & process the raw data and plot each panel in Figure 13)
- Plotting scripts for Figure 14 (Gnuplot scripts in .gnu that read & process the raw data and plot each panel in Figure 14)
- Plotting scripts for Figure 15 (Gnuplot scripts in .gnu that read & process the raw data and plot each panel in Figure 15)
- Plotting scripts for Figure 16 (Gnuplot scripts in .gnu that read & process the raw data and plot each panel in Figure 16)
- Plotting script for Figure 17 (Gnuplot script in .gnu that reads & processes the raw data and plots each panel in Figure 17)
- Plotting script for Figure 19 (Gnuplot script in .gnu that reads & processes the raw data and plots each panel in Figure 19)

Software availability

A third-party proprietary software, Ansys®Electronics Desktop 2018.1.0 (Release 19.1.0), was used to obtain the electromagnetic properties of the film under study, such as the wavelength, insertion loss, wave vector and characteristic impedance tabulated in the manuscript and the dataset listed in the *Data availability* statement. Due to the complexity of Ansys®Electronics Desktop, there are no freely available open source alternatives to replace the full functionality of this *em* software and that can perform the same simulation (to our knowledge). Nevertheless, we have described the primary methodology behind the software and have provided the associated output data and analysis code.

Ethics and consent

Ethical approval and consent were not required.

Acknowledgements

F. Boussaha and C. Chaumont acknowledge the supports from Paris Observatory and Paris Science and Lettre (PSL) University, of which they are the leader of the research and development group and clean room process engineer, respectively. The authors also would like to thank Florent Reix for helps in wafer cutting, and Ian Heywood for proof-reading the article.

References

1. Pospieszalski MW, Weinreb S, Norrod RD, *et al.*: **FETs and HEMTs at cryogenic temperatures-their properties and use in low-noise amplifiers.** *IEEE Trans Microw Theory Tech.* 1988; **36**(3): 552–560.
Publisher Full Text

2. Samoska LA: **An overview of solid-state integrated circuit amplifiers in the submillimeter-wave and THz regime.** *IEEE Trans Terahertz Sci Technol.* 2011; **1**(1): 9–24.
Publisher Full Text

3. Ajayan J, Nirmal D, Mathew R, *et al.*: **A critical review of design and fabrication challenges in InP HEMTs for future terahertz frequency applications.** *Mater Sci Semicond Process.* 2021; **128**: 105753.
Publisher Full Text

4. Aumentado J: **Superconducting parametric amplifiers: The state of the art in Josephson parametric amplifiers.** *IEEE Microw Mag.* 2020; **21**(8): 45–59.
Publisher Full Text

5. Grebel J, Bienfait A, Dumur É, *et al.*: **Flux-pumped impedance-engineered**

broadband Josephson parametric amplifier. *Appl Phys Lett.* 2021; **118**(14): 142601.
Publisher Full Text

6. Roy T, Kundu S, Chand M, *et al.*: **Broadband parametric amplification with impedance engineering: Beyond the gain-bandwidth product.** *Appl Phys Lett.* 2015; **107**(26): 262601.
Publisher Full Text

7. Eom BH, Day PK, LeDuc HG, *et al.*: **A wideband, low-noise superconducting amplifier with high dynamic range.** *Nat Phys.* 2012; **8**(8): 623–627.
Reference Source

8. Macklin C, O'Brien K, Hover D, *et al.*: **A near-quantum-limited Josephson traveling-wave parametric amplifier.** *Science.* 2015; **350**(6258): 307–310.
PubMed Abstract | Publisher Full Text

9. Malnou M, Aumentado J, Vissers MR, *et al.*: **Performance of a Kinetic Inductance Traveling-Wave Parametric Amplifier at 4 Kelvin: Toward an Alternative to Semiconductor Amplifiers.** *Phys Rev Appl.* 2022; **17**(4): 044009.
Publisher Full Text

10. Giachero A, Barone C, Borghesi M, *et al.*: **Detector Array Read-out with Traveling Wave Amplifiers**. *arXiv preprint arXiv: 2111.01512*. 2021.
Reference Source

11. Esposito M, Ranadive A, Planat L, *et al.*: **Perspective on traveling wave microwave parametric amplifiers.** *Appl Phys Lett.* 2021; **119**(12): 120501.
Publisher Full Text

12. Zobrist N, Eom BH, Day P, *et al.*: **Wide-band parametric amplifier readout and resolution of optical microwave kinetic inductance detectors.** *Appl Phys Lett.* 2019; **115**(4): 042601.
Publisher Full Text

13. Su FF, Wang ZT, Xu HK, *et al.*: **Nb-based Josephson parametric amplifier for superconducting qubit measurement.** *Chinese Phys B.* 2019; **28**(11): 110303.
Reference Source

14. Kundu S, Gheeraert N, Hazra S, *et al.*: **Multiplexed readout of four qubits in 3D circuit QED architecture using a broadband Josephson parametric amplifier.** *Appl Phys Lett.* 2019; **114**(17): 172601.
Publisher Full Text

15. Harris CT, Lu TM, Miller AJ, *et al.*: **Towards Quantum-Limited Cryogenic Amplification for Multi-Qubit Platforms**. Technical report, Sandia National Lab.(SNL-NM), Albuquerque, NM (United States), 2019.
Reference Source

16. Ranzani L, Bal M, Fong KC, *et al.*: **Kinetic inductance traveling-wave amplifiers for multiplexed qubit readout.** *Appl Phys Lett.* 2018; **113**(24): 242602.
Publisher Full Text

17. Braine T, Cervantes R, Crisosto N, *et al.*: **Extended search for the invisible axion with the axion dark matter experiment.** *Phys Rev Lett.* 2020; **124**(10): 101303.
PubMed Abstract | Publisher Full Text

18. Kutlu C, van Loo AF, Uchaikin SV, *et al.*: **Characterization of a flux-driven Josephson parametric amplifier with near quantum-limited added noise for axion search experiments.** *Supercond Sci Technol.* 2021; **34**(8): 085013.
Publisher Full Text

19. Bartram C, Braine T, Cervantes R, *et al.*: **Dark Matter Axion Search Using a Josephson Traveling Wave Parametric Amplifier**. *arXiv preprint arXiv: 2110.10262*. 2021.
Reference Source

20. Vissers MR, Erickson RP, Ku HS, *et al.*: **Low-noise kinetic inductance traveling-wave amplifier using three-wave mixing.** *Appl Phys Lett.* 2016; **108**(1): 012601.
PubMed Abstract | Publisher Full Text | Free Full Text

21. Bockstiegel C, Gao J, Vissers MR, *et al.*: **Development of a broadband NbTiN traveling wave parametric amplifier for MKID readout.** *J Low Temp Phys.* 2014; **176**(3): 476–482.
Publisher Full Text

22. Chaudhuri S, Li D, Irwin KD, *et al.*: **Broadband parametric amplifiers based on nonlinear kinetic inductance artificial transmission lines.** *Appl Phys Lett.* 2017; **110**(15): 152601.
Publisher Full Text

23. Malnou M, Vissers MR, Wheeler JD, *et al.*: **Three-wave mixing kinetic inductance traveling-wave amplifier with near-quantum-limited noise performance.** *PRX Quantum.* 2021; **2**(1): 010302.
Publisher Full Text

24. Shan W, Sekimoto Y, Noguchi T: **Parametric amplification in a superconducting microstrip transmission line.** *IEEE Trans Appl Supercond.* 2016; **26**(6): 1–9.
Publisher Full Text

25. Shu S, Klimovich N, Eom BH, *et al.*: **Nonlinearity and wide-band parametric amplification in a (Nb, Ti)N mi-crostrip transmission line.** *Phys Rev Res.* 2021; **3**(2): 023184.
Publisher Full Text

26. Goldstein S, Kirsh N, Svetitsky E, *et al.*: **Four wave-mixing in a microstrip kinetic inductance travelling wave parametric amplifier.** *Appl Phys Lett.* 2020; **116**(15): 152602.
Publisher Full Text

27. Adamyan AA, De Graaf SE, Kubatkin SE, *et al.*: **Superconducting microwave parametric amplifier based on a quasi-fractal slow propagation line.** *J Appl Phys.* 2016; **119**(8): 083901.
Publisher Full Text

28. Longden J, Boussaha F, Chaumont C, *et al.*: **Preliminary characterisation of titanium nitride thin film at 300 mK for the development of kinetic inductance travelling wave parametric amplifiers**. In *Quantum Technology: Driving Commercialisation of an Enabling Science II*. SPIE, 2021; **11881**: 130–138.
Publisher Full Text

29. Yaakobi O, Friedland L, Macklin C, *et al.*: **Parametric amplification in Josephson junction embedded transmission lines.** *Phys Rev B.* 2013; **87**(14): 144301.
Publisher Full Text

30. White TC, Mutus JY, Hoi IC, *et al.*: **Traveling wave parametric amplifier with Josephson junctions using minimal resonator phase matching.** *Appl Phys Lett.* 2015; **106**(24): 242601.
Publisher Full Text

31. O'Brien K, Macklin C, Siddiqi I, *et al.*: **Resonant phase matching of Josephson junction traveling wave parametric amplifiers.** *Phys Rev Lett.* 2014; **113**(15): 157001.
PubMed Abstract | Publisher Full Text

32. Simbierowicz S, Vesterinen V, Milem J, *et al.*: **Characterizing cryogenic amplifiers with a matched temperature-variable noise source.** *Rev Sci Instrum.* 2021; **92**(3): 034708.
PubMed Abstract | Publisher Full Text

33. Tan BK, Yassin G: **Design of a uniplanar resonance phase-matched Josephson traveling-wave parametric amplifier**. In: *2017 10th UK-Europe-China Workshop on Millimetre Waves and Terahertz Technologies (UCMMT)*. IEEE, 2017; 1–4.
Publisher Full Text

34. Ratter K, Tan BK: **A dispersion-engineered Josephson travelling wave parametric amplifier with periodic impedance perturbation**. In: *Proceeding of 32nd International Symposium on Space Terahertz Technology (ISSTT)*. 2021.
Reference Source

35. Navarro JM, Tan BK: **Optimising the design of a broadband Josephson junction TWPA for axion dark matter search experiments**. In *Quantum Technology: Driving Commercialisation of an Enabling Science II*. SPIE, 2021; **11881**: 139–148.
Publisher Full Text

36. Chaudhuri S, Gao J, Irwin K: **Simulation and analysis of superconducting traveling-wave parametric amplifiers.** *IEEE Trans Appl Supercond.* 2014; **25**(3): 1–5.
Publisher Full Text

37. Zhao S, Withington S, Goldie DJ, *et al.*: **Loss and saturation in superconducting travelling-wave parametric amplifiers.** *J Phys D Appl Phys.* 2019; **52**(41): 415301.
Publisher Full Text

38. Valenzuela D, Mena FP, Baselmans J: **Modelling dielectric losses in microstrip traveling-wave kinetic-inductance parametric amplifiers.** In *30th International Symposium on Space THz Technology* (Gothenburg, Sweden), 2019; 63–66.

39. Zmuidzinas J: **Superconducting Microresonators: Physics and Applications.** *Annu Rev Condens Matter Phys.* 2012; **3**(1): 169–214.
Publisher Full Text

40. Zorin AB: **Josephson traveling-wave parametric amplifier with three-wave mixing.** *Phys Rev Appl.* 2016; **6**(3): 034006.
Publisher Full Text

41. Sivak VV, Frattini NE, Joshi VR, *et al.*: **Kerr-free three-wave mixing in superconducting quantum circuits.** *Phys Rev Applied.* 2019; **11**(5): 054060.
Publisher Full Text

42. Sweetnam T, Banys D, Gilles V, *et al.*: **Simulating the behaviour of travelling wave superconducting parametric amplifiers using a commercial circuit simulator**. *arXiv preprint arXiv: 2203.09660*. 2022.
Reference Source

43. Mattis DC, Bardeen J: **Theory of the anomalous skin effect in normal and superconducting metals.** *Phys Rev.* 1958; **111**(2): 412.
Publisher Full Text

44. Zhao S, Goldie DJ, Thomas CN, *et al.*: **Calculation and measurement of critical temperature in thin superconducting multilayers.** *Supercond Sci Technol.* 2018; **31**(10): 105004.
Publisher Full Text

45. Kher A, Day PK, Eom BH, *et al.*: **Kinetic inductance parametric up-converter.** *J Low Temp Phys.* 2016; **184**(1): 480–485.
Publisher Full Text

46. Zhao S, Withington S: **Quantum analysis of second-order effects in superconducting travelling-wave parametric amplifiers.** *J Phys D Appl Phys.* 2021; **54**(36): 365303.
Publisher Full Text

47. De Visser PJ: **Quasiparticle dynamics in aluminium superconducting microwave resonators**. PhD thesis, Delft University of Technology (TU Delft), 2014.
Publisher Full Text

48. Boussaha F: **personal communication**. 2021.

49. Glowacka DM, Goldie DJ, Withington S, *et al.*: **Development of a NbN deposition process for superconducting quantum sensors**. *arXiv preprint arXiv: 1401.2292*. 2014.
Publisher Full Text

50. Boussaha F, Beldi S, Monfardini A, *et al.*: **Development of TiN Vacuum-Gap Capacitor Lumped-Element Kinetic Inductance Detectors.** *J Low Temp Phys.* 2020; **199**(3): 994–1003.
Publisher Full Text

51. Tan BK: **Engineering the Thin Film Characteristics for Optimal Performance of Superconducting Kinetic Inductance Amplifiers using a Rigorous Modelling Technique**. *figshare*. Dataset. 2022.
http://www.doi.org/10.6084/m9.figshare.c.6034133.v1

52. Li D, Gao J, Austermann JE, *et al.*: **Improvements in silicon oxide dielectric loss for superconducting microwave detector circuits.** *IEEE Trans Appl Supercond.* 2013; **23**(3): 1501204.
Publisher Full Text

53. O'Connell AD, Ansmann M, Bialczak RC, *et al.*: **Microwave dielectric loss at single photon energies and millikelvin temperatures.** *Appl Phys Lett.* 2008; **92**(11): 112903.
Publisher Full Text

Open Peer Review

Current Peer Review Status: ✔ ✔ ✔

Version 2

Reviewer Report 12 October 2023

https://doi.org/10.21956/openreseurope.17916.r35100

Fausto Patricio Mena
[1] Electrical Engineering Department, University of Chile, Santiago, Chile
[2] National Radio Astronomy Observatory, Charlottesville, VA, USA

The authors have addressed all my comments. No further revision is needed.

Competing Interests: No competing interests were disclosed.

I confirm that I have read this submission and believe that I have an appropriate level of expertise to confirm that it is of an acceptable scientific standard.

Reviewer Report 02 October 2023

https://doi.org/10.21956/openreseurope.17916.r35102

Wenlei Shan
Advanced Technology Center (ATC), National Astronomical Observatory of Japan (NAOJ), Tokyo, Japan

The authors have responded to all the comments that I made and made necessary modifications in the revision. I suggest approval of this version.

Competing Interests: No competing interests were disclosed.

Reviewer Expertise: Superconducting electronics, Radio Astronomical Techniques

I confirm that I have read this submission and believe that I have an appropriate level of expertise to confirm that it is of an acceptable scientific standard.

Reviewer Report 22 September 2023

https://doi.org/10.21956/openreseurope.17916.r35101

Martina Esposito
CNR, SPIN Institute, Naples, Italy

The authors satisfactory addressed all my previous comments and I have no further comments to make.

Competing Interests: No competing interests were disclosed.

Reviewer Expertise: superconducting quantum devices, traveling parametric amplifiers

I confirm that I have read this submission and believe that I have an appropriate level of expertise to confirm that it is of an acceptable scientific standard.

Version 1

Reviewer Report 15 November 2022

https://doi.org/10.21956/openreseurope.16055.r30185

Martina Esposito
CNR, SPIN Institute, Naples, Italy

The manuscript presents an interesting modelling method for KTWPA devices capturing the effect of both the adopted materials and the chosen topology by combining the use of 3D em-simulation software and the solution of coupled differential equations for the description of modes propagation.

First, the modelling methodology is presented. Subsequently, the authors focus on modelling different thin film materials and different transmission line topologies. Finally, two possible

designs are discussed in details and the results of model's predictions are compared with experimental results present in the literature.

The presented method is certainly interesting, and this work provides useful guidelines for designing KTWPAs.

However, in the present form, it results a bit difficult for the reader to catch the key results/achievements. Sections 3, 4 and 5 are very long with many figures, but probably some repetitions are present, for example different figures stressing similar aspects. I think the manuscript could strongly benefit from a careful revision with the aim to emphasising more the main results and summarizing in a more concise way the secondary aspects.

Specific comments are given below:

Abstract and Summary

I don't think it appropriate to define KTWPAs as a "new" variant of superconducting amplifiers, considering that the first device obtained with modern nanofab methods was demonstrated in 2012: Nat. Phys. 8, 623–627 (2012).

Summary

"As the amplifier is formed using the superconducting thin". Please check language/grammar.

Introduction

The list of references for experimentally demonstrated JTWPAs is not updated. Please check and possibly update the reference list according to state-of-the-art.

Methods

"If a weak signal at frequency Ω is detected". Confusing wording here: in order to get amplification, a weak signal should be 'applied' at input before being 'detected' at output.

Page 4 (end of first column): please check the correct use of punctuation, here and for the entire manuscript.

Page 5: it would be interesting if the authors could provide more details on the computation time typically required for the full modelling of the single unit cell.

Page 5: in order to obtain the results reported in the figures of section 5, are equation (3) and (4) solved numerically? Or, an analytic solution, under certain conditions, is adopted? This is a very interesting aspect; however, it is not very clear in my opinion in the manuscript and should be clarified.

Fig 1: one may deduce that a second loading section is also included in the design, however this does not appear in Fig 1 sketch (only first and third loading sections are mentioned), can the

authors please clarify?

Page 6: how is the contribution from the L_{geo} estimated?

Methods: could the modelling method explained in section 2 be adapted for JTWPAs? it would be interesting if the authors could comment about this possibility.

Please check that when an acronym is used for the first time, the definition is also reported. Example (MIKIDs in page 7).

Page 7: “From the plot, it clearly indicates that”. Please check language/grammar.

Section 3

How are plots (continuous lines) in fig from 2 to 8 obtained? If analytical expressions are used, can the authors please explicitly report the adopted analytical expressions for R_s, L_s and p_s? Reporting the analytical expressions could help in possibly removing some of the figures (especially the ones showing secondary aspects, that can be equivalently well described with a formula).

Fig 6: The authors should add or at least discuss error bars for the experimental points.

Page 10 “Therefore, it would be indicative to perform the same analysis at a fixed operational frequency instead of fractional frequency”. I totally agree with this. The authors could indeed focus directly on this kind of analysis (at fixed operational frequency) which is the useful one for the designing a device in a given frequency range. This will probably help in making the manuscript shorter and it will be easier for the reader to appreciate the key results.

Not necessary to repeat the acronym definition, the authors can define it just the first time that the acronym is used (general comment for all the manuscript). Example (KITWPA).

Page 16: “Therefore, we are confident that our proposed method can accurately predicts the gain-bandwidth performance of a KITWPA.” Very nice benchmark of the method. Does the same kind of validation check work for micro-strip geometries?

Section 5.3

Is the adopted modelling method considering the frequency-dependence of dielectric losses? Can the authors please give more details of this aspect? This is particularly relevant for the micro-strip geometry.

Section 5.3 “if the signal-to-noise ratio of the incoming signal can be estimated a priori.” What does this exactly mean? How do the authors suggest doing that?

Page 22 (last paragraph in first column): This sentence is confusing, please check.

Fig. 19: Very interesting comparison!

Page 25: it would be useful if the authors could discuss this noise comparison also in terms of expected number of photons above the standard quantum limit for the TWPA added noise.

Page 25: The authors should be careful when comparing theoretical prediction with experimental results. For example, instead of using the expression “successfully achieve” I believe it would be more appropriate to say "are predicted to achieve"/"are expected to achieve" or similar expressions. I have the same language comment for the subsequent comparison with ref 22 and 7, since in the current manuscript no experimental data are presented.

Last paragraph of section 5: Please check language/grammar.

Is the work clearly and accurately presented and does it cite the current literature?
Partly

Is the study design appropriate and does the work have academic merit?
Yes

Are sufficient details of methods and analysis provided to allow replication by others?
Yes

If applicable, is the statistical analysis and its interpretation appropriate?
Not applicable

Are all the source data underlying the results available to ensure full reproducibility?
Yes

Are the conclusions drawn adequately supported by the results?
Yes

Competing Interests: No competing interests were disclosed.

Reviewer Expertise: superconducting quantum devices, traveling parametric amplifiers

I confirm that I have read this submission and believe that I have an appropriate level of expertise to confirm that it is of an acceptable scientific standard, however I have significant reservations, as outlined above.

Author Response 01 Sep 2023

Boon Kok Tan

Dear Dr. Esposito, Thank you for taking your time to review the article thoroughly. My sincere apology for the long delay in responding. The responses for all your very useful comments are as below:

The manuscript presents an interesting modelling method for KTWPA devices capturing the effect of both the adopted materials and the chosen topology by combining the use of 3D

em-simulation software and the solution of coupled differential equations for the description of modes propagation.

First, the modelling methodology is presented. Subsequently, the authors focus on modelling different thin film materials and different transmission line topologies. Finally, two possible designs are discussed in details and the results of model's predictions are compared with experimental results present in the literature.

The presented method is certainly interesting, and this work provides useful guidelines for designing KTWPAs.

However, in the present form, it results a bit difficult for the reader to catch the key results/achievements. Sections 3, 4 and 5 are very long with many figures, but probably some repetitions are present, for example different figures stressing similar aspects. I think the manuscript could strongly benefit from a careful revision with the aim to emphasising more the main results and summarizing in a more concise way the secondary aspects.

Specific comments are given below:

Abstract and Summary

I don't think it appropriate to define KTWPAs as a "new" variant of superconducting amplifiers, considering that the first device obtained with modern nanofab methods was demonstrated in 2012: Nat. Phys. 8, 623–627 (2012).
Response: Removed.

Summary

"As the amplifier is formed using the superconducting thin". Please check language/grammar.
Response: Corrected.

Introduction

The list of references for experimentally demonstrated JTWPAs is not updated. Please check and possibly update the reference list according to state-of-the-art.

Methods

"If a weak signal at frequency Ω is detected". Confusing wording here: in order to get amplification, a weak signal should be 'applied' at input before being 'detected' at output.
Response: It depends on application. For used as first stage detector such as in astronomy, the signal is indeed detected. But nevertheless, corrected to 'applied'.

Page 4 (end of first column): please check the correct use of punctuation, here and for the entire manuscript.

Response: Done.

Page 5: it would be interesting if the authors could provide more details on the computation time typically required for the full modelling of the single unit cell.
Response: It varies between the many different topologies investigated here. It also depends on the meshing methods etc, but generally could be between tens of minutes to several hours.

Page 5: in order to obtain the results reported in the figures of section 5, are equation (3) and (4) solved numerically? Or, an analytic solution, under certain conditions, is adopted? This is a very interesting aspect; however, it is not very clear in my opinion in the manuscript and should be clarified.
Response: It's written in the text that these CMEs are solved numerically. Analytical solutions can be sought using the undepleted pump assumption as state in the text, but the procedures are rather standard but too lengthy to be included here (which can be found in the citation included), and is not important to the investigation we wish to perform here, which needs to include the effect of losses in the pump power.

Fig 1: one may deduce that a second loading section is also included in the design, however this does not appear in Fig 1 sketch (only first and third loading sections are mentioned), can the authors please clarify?
Response: We follow the convention used by Eom et. al. 2012, the very first paper that describe the scheme. The second loading section is in fact identical to the first, hence generally in the field, the loading are denoted as first loading and third loading to differentiate the two.

Page 6: how is the contribution from the L_{geo} estimated?
Response: This was explained in the second box of Fig. 1, where we remove the superconductivity boundary condition of the model and calculate the wave vector which is then subtracted from the total wave vector of the model that include superconductivity.

Methods: could the modelling method explained in section 2 be adapted for JTWPAs? it would be interesting if the authors could comment about this possibility.
Response: Yes, indeed! We are currently preparing a paper to describe this effort.

Please check that when an acronym is used for the first time, the definition is also reported. Example (MIKIDs in page 7).
Response: The acronym is already explained at the end of introduction.

Page 7: “From the plot, it clearly indicates that”. Please check language/grammar.
Response: We believed this is fine.

Section 3

How are plots (continuous lines) in fig from 2 to 8 obtained? If analytical expressions are used, can the authors please explicitly report the adopted analytical expressions for ,

R_s, L_s and ρ_s? Reporting the analytical expressions could help in possibly removing some of the figures (especially the ones showing secondary aspects, that can be equivalently well described with a formula).
Response: It's calculated numerically using the Mattis-Bardeen equation which was explained in Section 2 and cited the source.

Fig 6: The authors should add or at least discuss error bars for the experimental points.
Response: We don't have the information of the error bars for Fig.6a, as it is a one-off measurement that takes a large effort to perform experimentally.

Page 10 "Therefore, it would be indicative to perform the same analysis at a fixed operational frequency instead of fractional frequency". I totally agree with this. The authors could indeed focus directly on this kind of analysis (at fixed operational frequency) which is the useful one for the designing a device in a given frequency range. This will probably help in making the manuscript shorter and it will be easier for the reader to appreciate the key results.
Response: Thanks. Equally, many peers would argue that it is easier to understand the analysis using fractional frequency. Therefore, we showed both for better comparison.

Not necessary to repeat the acronym definition, the authors can define it just the first time that the acronym is used (general comment for all the manuscript). Example (KITWPA).
Response: If the reviewer is referring to the repeated acronym definitions in the caption of figures and table, this is unfortunately the requirement from the journal, which is beyond the control of the authors.

Page 16: "Therefore, we are confident that our proposed method can accurately predicts the gain-bandwidth performance of a KITWPA." Very nice benchmark of the method. Does the same kind of validation check work for micro-strip geometries?
Response: Thanks. Indeed, for microstrip as well. We report the validation in a separate article.

Section 5.3

Is the adopted modelling method considering the frequency-dependence of dielectric losses? Can the authors please give more details of this aspect? This is particularly relevant for the micro-strip geometry.
Response: Yes, it does. This is clearly shown Fig.17(b), and explained in Section 5.4 which focuses on the microstrip geometry.

Section 5.3 "if the signal-to-noise ratio of the incoming signal can be estimated a priori." What does this exactly mean? How do the authors suggest doing that?
Response: This section has been removed.

Page 22 (last paragraph in first column): This sentence is confusing, please check.
Response: Done.

Fig. 19: Very interesting comparison!
Response: Thanks.

Page 25: it would be useful if the authors could discuss this noise comparison also in terms of expected number of photons above the standard quantum limit for the TWPA added noise.
Response: This paper focuses on the design consideration of KITWPA from the perspective of electromagnetism and thin film properties. The noise performance is a related but a different and important topic that needs equally in-depth investigations, which is beyond the scope of this paper.

Page 25: The authors should be careful when comparing theoretical prediction with experimental results. For example, instead of using the expression “successfully achieve” I believe it would be more appropriate to say "are predicted to achieve"/"are expected to achieve" or similar expressions. I have the same language comment for the subsequent comparison with ref 22 and 7, since in the current manuscript no experimental data are presented.
Response: Corrected.

Competing Interests: No competing interests were disclosed.

Reviewer Report 15 November 2022

https://doi.org/10.21956/openreseurope.16055.r30186

?

Wenlei Shan
Advanced Technology Center (ATC), National Astronomical Observatory of Japan (NAOJ), Tokyo, Japan

This manuscript describes simulation, material properties, transmission line configuration, and design consideration of kinetic inductance traveling wave parametric amplifiers (TPAs). It is a comprehensive paper covering important aspects of development of TPAs, which is now gaining intensive interests both in quantum computing and week signal detection in astronomical observation. The applications will be more broadened with further revealing their features and potential. In this study, the authors established an improved simulation method by involving commercial EM simulator and, therefore, they can deal with circuit with various structures more realistically than before. They obtained new understandings in the selection of superconducting materials and transmission line configuration. With this set of new tools and consideration, they finished two designs of TPAs, which are expected to show superior performance. Apparently, this paper is valuable to the researchers who are doing study in this field.

This review report will focus on some points that should be improved in the way of presenting or should be further explained or analyzed. The manuscript can be better understood and more helpful to the society if these points are strengthened. The followings are major ones.

1. Section 2, Methods. Equation (3) seems to be problematic. The equations should reduce to trivial ones dA/dz=0 if the nonlinearity approaches to zero. Normally, there should be the nonlinear factor on the left side of each equation, which is proportional to $(I_p/I_0)^2$, where Ip and I_0 are pump current and critical current of the conducting strip respectively. But the nonlinear factor is not found in Equation (3).

2. Section 2, Methods. The sequence of TPA simulation is explained in Figure 1. It is not difficult to understand how the ABCD matrix of each unit cell is obtained by using EM simulation. But it is not clear how these linear matrixes are combined with the coupled equations to calculate the gain-bandwidth profile of the TPA. It is obvious that the explanation of solving the nonlinear equations is missing. Readers will be unable to reproduce this calculation without knowing the method of solving the equations.

3. Section 2, All R_S in the text and the figures are in unit of *kΩ/sq*. They are unreasonably large sheet resistance and, therefore, the unit must be mistaken.
4. Section 2, the ratio of surface inductance to resistance, L_S/R_S , is used as a figure of merit in selection of material for TPAs. This is reasonable if microstrip (MS) is used as the transmission line because the differential inductance of the line is dominated by L_S. But for CPW, the geometric inductance is significant, therefore the propagation constant is less influenced by L_S as in MS. In this case, the ratio of total inductance to Rs should be a better choice.
5. Section 2, Figure 5 presents the most important result that lead to one of the key conclusions of this paper, i.e. film normal state resistivity is not very critical in selection of material for TPAs. The authors consider these results are “rather unexpected”. At least, the observation of $L_s \propto \rho_N/V_{gap}$ can be explained in the following way. In the case of thin film, where the thickness is much less than the penetration depth, the film sheet impedance is approximately:

$Z_s = \frac{1}{(\sigma_1 - j\sigma_2)t} = R_s + jX_s$. For the complex conductivity $\sigma = \sigma_1 - j\sigma_2$ of a superconductor, usually the real part is much smaller than the imaginary part. Then the surface resistance and reactance are approximated as $X_s = \omega L_s = \frac{1}{\sigma_2 t}$, $R_s = X_s \frac{\sigma_1}{\sigma_2}$ and , where t is the film thickness. The imaginary part of the conductivity can be expressed by using the energy gap for the (BCS) superconductor as $\frac{\sigma_1}{\sigma_n} = \frac{\pi\Delta}{\hbar\omega}$, where σ_n is normal state conductivity of the thin film, and Δ is the energy gap. Then the surface inductance L_s can be expressed by energy gap and normal state resistivity $\rho_n = \frac{1}{\sigma_n}$ as $L_s = \frac{\hbar\rho N}{\Delta\pi t}$. It is independent of frequency, proportional to film's normal state resistivity and reversely proportional to the energy gap. This is what is observed in Figure 5 b. However, from this analysis, R_S is also proportional to ρN instead of $\rho^2 N$ as observed in Figure 5 a. So, there is

a contradiction between the theory presented here and the simulation result in Figure 5 (a) in the paper. Since the authors found the rule $R_s \propto \rho^2 N$ from calculation, there must be a corresponding theory supporting it. It is necessary to provide the theoretical explanation of this key result and prove my analysis is wrong, which show a linear dependence.

6. The ohmic loss of superconducting thin films are strongly dependent on the operating temperature. There are general missing of mentioning temperature information, at which the calculations were performed. This is a serious problem of the present version of this paper.

7. The authors claim that if the film thickness can be controlled accurately the selection of material is not critical. Because the film quality (for example the critical temperature) is dependent on the thickness especially when the film is very thin, only accurate thickness is not sufficient, and other properties much be maintained.

8. The loss of transmission line is applied to the signal in the simulation. This makes the study more realistic than those where transmission loss is neglected. However, it is not clearly mentioned in the text whether the loss is also applied to the pump. Because the nonlinearity of the line is strongly dependent on the pumping strength, the dissipation of pump significantly affects the performance when the transmission line is physically long. Please clarify this point or add proper analysis on the impact of gradually weakening of the pump along the line.

Followings are minor comments:

Page 3, left column, line 11. "...using the superconducting thin, we investigate..." missing word "film".

Page 3, right column, line 3. "In order to increase the interaction time." Please explain the definition of "interaction time" or provide a reference.

Page 4, left column, line 12. "... amplified to preserve the total momentum of the system." Please explain "momentum of the system" or provide a reference.

Page 4, above equation (3), "Substituing the propagating wave into Equation 2, assuming that ...", please explain why these assumptions are reasonable especially the second one or provide references.

Page 5, left column, line 10 from bottom. "However, this approach neglects many subtle effects that could arise from cascading hundreds of these unit cells..." what are those subtle effects? or provide a reference.

Page 6, left column, the final line. "... which assume the kinetic inductance of the thin film is dominating in the case of TPA and hence the geometric inductance of the STL is neglected in the calculation..." What is neglected in most of calculations is the magnetic field penetration into the film rather than that in dielectric media. Because films are normally thin, much thinner than the geometric scale of dielectric layer, the neglection of this part will not introduce significant effect. It is only a very small part of "geometric inductance".

Page 13, left column, line 9 from bottom. "... using silicon monoxide (SiO) with a resistivity ... loss tangent 0.004...". The loss of SiO used here is obvious much larger than the more conventional used material SiO_2. Please explain the reason of making use of lossy material here.

Page 15, left column, line 15. "Hence, even with a very high substrate resistivity of $\rho = 15k\Omega cm$, the losses are still visibly higher due to the long transmission length." What is the resistivity at cryogenic temperature? Most of thermally activated charges will get frozen at operation temperature.

Page 16, Figure 10. It is recommended to show a complete unit and specify (by labeling) the first and third loading sections and primary section corresponding to Figure 1.

Page 17, Figure 11 (b). It is recommended that the relative phase error Δϕ/ϕ should be used rather than the absolute value because the overall lengths are different in this comparison.

Page 21, left column, line 17. "Although generally one would assume that the amplifier should operate below the compression point, but this is not necessarily the case as long as there is still parametric gain; but the amplifier is not operating in the linear regime anymore." This sentence does not make sense to me.

Page 21, Table 5. Please add the information of the total length of the line, for which the losses are calculated.

Page 24, Figure 18. The bridges cannot be clearly seen. An enlarged view is necessary.

Page 25, left column, line 4. "we can estimate the noise power via I2rmsR." Is it better to use the thermal noise temperature $T_n \approx \alpha L T k_B B \approx Z_0 R_s L k_B T$, where L is the length, α is the real part of propagation constant, k_B is Boltzmann constant and T is the physical temperature? It is not clear to me why the pump power is relevant.

Page 25, right column, line 2 from bottom. "...but in order to minimize cross talk..." cross talk issue is not discussed in this paper. It is suggested to add analysis on cross talk, which will be interesting.

Is the work clearly and accurately presented and does it cite the current literature?
Partly

Is the study design appropriate and does the work have academic merit?
Yes

Are sufficient details of methods and analysis provided to allow replication by others?
Partly

If applicable, is the statistical analysis and its interpretation appropriate?
Not applicable

Are all the source data underlying the results available to ensure full reproducibility?
Partly

Are the conclusions drawn adequately supported by the results?
Partly

Competing Interests: No competing interests were disclosed.

Reviewer Expertise: Superconducting electronics, Radio Astronomical Techniques

I confirm that I have read this submission and believe that I have an appropriate level of expertise to confirm that it is of an acceptable scientific standard, however I have significant reservations, as outlined above.

Author Response 01 Sep 2023

Boon Kok Tan

Dear Prof. Shan, Thank you for taking your time to review the article thoroughly. My sincere apology for the long delay in responding. The responses for all your very useful comments are as below:

This manuscript describes simulation, material properties, transmission line configuration, and design consideration of kinetic inductance traveling wave parametric amplifiers (TPAs). It is a comprehensive paper covering important aspects of development of TPAs, which is now gaining intensive interests both in quantum computing and week signal detection in astronomical observation. The applications will be more broadened with further revealing their features and potential. In this study, the authors established an improved simulation method by involving commercial EM simulator and, therefore, they can deal with circuit with various structures more realistically than before. They obtained new understandings in the selection of superconducting materials and transmission line configuration. With this set of new tools and consideration, they finished two designs of TPAs, which are expected to show superior performance. Apparently, this paper is valuable to the researchers who are doing study in this field.

This review report will focus on some points that should be improved in the way of presenting or should be further explained or analyzed. The manuscript can be better understood and more helpful to the society if these points are strengthened. The followings are major ones.

1. Section 2, Methods. Equation (3) seems to be problematic. The equations should reduce to trivial ones dA/dz=0 if the nonlinearity approaches to zero. Normally, there should be the nonlinear factor on the left side of each equation, which is proportional to $(I_p / I_0)^2$, where I_p and I_0 are pump current and critical current of the conducting strip respectively. But the nonlinear factor is not found in Equation (3).

   Response: This is a very standard sets of coupled mode equation (CME) used widely for predicting the gain performance of KITWPA, except that we include the loss factor (\alpha) in the propagation constant (\gamma). See for example Eom et. al. 2012 for

the similar derivation. The parameter Ip is directly related to the Ap in the equation.

2. Section 2, Methods. The sequence of TPA simulation is explained in Figure 1. It is not difficult to understand how the ABCD matrix of each unit cell is obtained by using EM simulation. But it is not clear how these linear matrixes are combined with the coupled equations to calculate the gain-bandwidth profile of the TPA. It is obvious that the explanation of solving the nonlinear equations is missing. Readers will be unable to reproduce this calculation without knowing the method of solving the equations.

   Response: As mentioned in the article, the unit cells are cascaded using transfer matrix method, which is a commonly used method. Basically, it's just a dot-matrix product of the unit cells. This can be easily done using commercial or standard circuit emulators, or by writing a simple python code to do the matrix product. As pointed out in the text and in Fig.1, one can easily extract the propagation constant (\gamma) using the cascaded ABCD matrix, which are available in many electromagnetisms' textbook e.g., Pozar's Microwave Engineering. The CME noted in the article can then be solved numerically using python, Mathematica, Matlab or any other numerical software one prefers. As the article is focusing on the main message of the finding, these trivial step-by-step instructions would distract the focus of the reader on the scientific content of paper, hence not included. For these instructions, I invite you to look out for Joseph's thesis which should be published shortly after he completed his PhD.

3. Section 2, All R_S in the text and the figures are in unit of $k\Omega / sq$. They are unreasonably large sheet resistance and, therefore, the unit must be mistaken.
4.
   Response: Well spotted! Thanks for pointing that out. It was supposed to be mOhm not kOhm. All figures and texts are updated.

5. Section 2, the ratio of surface inductance to resistance, L_s / R_s , is used as a figure of merit in selection of material for TPAs. This is reasonable if microstrip (MS) is used as the transmission line because the differential inductance of the line is dominated by L_s . But for CPW, the geometric inductance is significant, therefore the propagation constant is less influenced by L_s as in MS. In this case, the ratio of total inductance to Rs should be a better choice.

   Response: As stated in the paper, the geometric inductance does not contribute to the wave-mixing process that promote amplification gain, hence it is more proper to use Ls instead of total inductance.
6. Section 2, Figure 5 presents the most important result that lead to one of the key conclusions of this paper, i.e. film normal state resistivity is not very critical in selection of material for TPAs. The authors consider these results are "rather unexpected". At least, the observation of $L_s \propto \rho_N / V_{gap}$ can be explained in the following way. In the case of thin film, where the thickness is much less than the penetration depth, the film sheet impedance is approximately:

$Z_s = \frac{1}{(\sigma_1 - j\sigma_2)t} = R_s + jX_s$. For the complex conductivity $\sigma = \sigma_1 - j\sigma_2$ of a superconductor, usually the real part is much smaller than the imaginary part. Then the surface resistance and reactance are approximated as $X_s = \omega L_s = \frac{1}{\sigma_2 t}$, and $R_s = X_s \frac{\sigma_1}{\sigma_2}$, where t is the film thickness. The imaginary part of the conductivity can be expressed by using the energy gap for the (BCS) superconductor as $\frac{\sigma_1}{\sigma_n} = \frac{\pi\Delta}{\hbar\omega}$, where σ_n is normal state conductivity of the thin film, and Δ is the energy gap. Then the surface inductance L_s can be expressed by energy gap and normal state resistivity $\rho_n = \frac{1}{\sigma_n}$ as $L_s = \frac{\hbar\rho N}{\Delta\pi t}$. It is independent of frequency, proportional to film's normal state resistivity and reversely proportional to the energy gap. This is what is observed in Figure 5 b. However, from this analysis, R_s is also proportional to ρN instead of $\rho^2 N$ as observed in Figure 5 a. So, there is a contradiction between the theory presented here and the simulation result in Figure 5 (a) in the paper. Since the authors found the rule $R_s \propto \rho^2 N$ from calculation, there must be a corresponding theory supporting it. It is necessary to provide the theoretical explanation of this key result and prove my analysis is wrong, which show a linear dependence.

Response: Thanks for pointing out the derivation. As you mentioned Rs=Xs(rho1/rho2). But as you pointed as well, there is an inverse relation between Xs and rho2, where rho2 = 1/(t Xs). If you replace this back to the Rs equation, it leads to Rs = rho1 t Xs^2 = rho1 t omega^2 Ls^2. Given that Ls is directly proportional to rhoN, you can see that in fact Rs is proportional to rhoN^2.

7. The ohmic loss of superconducting thin films are strongly dependent on the operating temperature. There are general missing of mentioning temperature information, at which the calculations were performed. This is a serious problem of the present version of this paper.

   Response: The operating temperature used for all the analysis presented in the paper is unchanged, and set at 10mK. This is highlighted at the end of the first paragraph of Section 3. We agree that the ohmic loss is dependent on the operating temperature, but to include the effect of various operating temperature is beyond the scope of this paper. A similar investigation on the effect of operating temperature can indeed be performed in the future.

8. The authors claim that if the film thickness can be controlled accurately the selection of material is not critical. Because the film quality (for example the critical temperature) is dependent on the thickness especially when the film is very thin, only accurate thickness is not sufficient, and other properties much be maintained.

Response: We agree with the statement. However, in this paper, we focus only on the aspect of electromagnetism and superconductivity that affecting the performance of TWPA. The topic of fabrication complication addressing the other properties such as uniformity of the film etc., is beyond the scope of this paper.

9. The loss of transmission line is applied to the signal in the simulation. This makes the study more realistic than those where transmission loss is neglected. However, it is not clearly mentioned in the text whether the loss is also applied to the pump. Because the nonlinearity of the line is strongly dependent on the pumping strength, the dissipation of pump significantly affects the performance when the transmission line is physically long. Please clarify this point or add proper analysis on the impact of gradually weakening of the pump along the line.

   Response: As shown in Eq.(3), the term \alpha_p which denote the loss on the pump term is not omitted throughout, hence the loss is also applied to the pump. Furthermore, in paragraph 5 of Section 2, it is clear that the general CME presented in Eq.(3) do take into account the loss of the pump, as we pointed out that this CME can be reduced using the undepleted pump assumption as special case. This is also quite clearly shown in Fig.11(c). Nevertheless, we add in a line at the end of paragraph 5 to clearly pointing out to the readers that the effect of loss on the pump is included in all the analyses.

Followings are minor comments:
Response: Thank you for your careful read of the article. Greatly appreciated.

Page 3, left column, line 11. "...using the superconducting thin, we investigate..." missing word "film".
Response: Done.

Page 3, right column, line 3. "In order to increase the interaction time." Please explain the definition of "interaction time" or provide a reference.
Response: As stated in the text, it is the interaction time between the pump and the signal tone within the nonlinear medium.

Page 4, left column, line 12. "... amplified to preserve the total momentum of the system." Please explain "momentum of the system" or provide a reference.
Response: There is no special definition of momentum used in the article, but the most basic notion of momentum used in all major physics textbook.

Page 4, above equation (3), "Substituing the propagating wave into Equation 2, assuming that ...", please explain why these assumptions are reasonable especially the second one or provide references.
Response: Reference provided.

Page 5, left column, line 10 from bottom. "However, this approach neglects many subtle effects that could arise from cascading hundreds of these unit cells..." what are those subtle effects? or provide a reference.

Response: Examples added.

Page 6, left column, the final line. "... which assume the kinetic inductance of the thin film is dominating in the case of TPA and hence the geometric inductance of the STL is neglected in the calculation..." What is neglected in most of calculations is the magnetic field penetration into the film rather than that in dielectric media. Because films are normally thin, much thinner than the geometric scale of dielectric layer, the neglection of this part will not introduce significant effect. It is only a very small part of "geometric inductance".
Response: We agree that the geometric inductance effect is minor in most cases, but it is more mathematically appropriate to include this effect in the calculation because the geometric inductance do not contribute to parametric gain, and may results in over-estimate the gain.

Page 13, left column, line 9 from bottom. "... using silicon monoxide (SiO) with a resistivity ... loss tangent 0.004...". The loss of SiO used here is obvious much larger than the more conventional used material SiO_2. Please explain the reason of making use of lossy material here.
Response: SiO is chosen here just as an example, the analysis of this section remains the same if one replace SiO with other dielectric material. The effect of dielectric material is subsequently investigated in Section 5.4.

Page 15, left column, line 15. "Hence, even with a very high substrate resistivity of $\rho = 15k\Omega cm$, the losses are still visibly higher due to the long transmission length." What is the resistivity at cryogenic temperature? Most of thermally activated charges will get frozen at operation temperature.
Response: Given that we do not possess the exact value of resistivity of various substrates at cryogenic temperature, it is difficult to perform the analysis with guess values for different substrates and hence resulting in misleading information. Nevertheless, we do agree that most thermally activated charges will get frozen to some degree at low operating temperature.

Page 16, Figure 10. It is recommended to show a complete unit and specify (by labeling) the first and third loading sections and primary section corresponding to Figure 1.
Response: Done.

Page 17, Figure 11 (b). It is recommended that the relative phase error $\Delta\phi/\phi$ should be used rather than the absolute value because the overall lengths are different in this comparison.
Response: One important key for maximising the gain is that the total phase mismatch delta_phi is closed to zero, and this behaviour changes with the length of the device, exactly the point we would like to address in this plot. Therefore, it is adamant to show the absolute value on where it crosses the zero-point.

Page 21, left column, line 17. "Although generally one would assume that the amplifier should operate below the compression point, but this is not necessarily the case as long as there is still parametric gain; but the amplifier is not operating in the linear regime anymore." This sentence does not make sense to me.

Response: This section has been removed.

Page 21, Table 5. Please add the information of the total length of the line, for which the losses are calculated.
Response: Added.

Page 24, Figure 18. The bridges cannot be clearly seen. An enlarged view is necessary.
Response: Done.
Page 25, left column, line 4. "we can estimate the noise power via a I2rmsR." Is it better to use the thermal noise temperature $T_n \approx \alpha L T k_B B \approx Z_0 R_s L k_B T$, where L is the length, α is the real part of propagation constant, k_B is Boltzmann constant and T is the physical temperature? It is not clear to me why the pump power is relevant.
Response: The majority of the current going through the TWPA is the pump, hence the relevance of pump power. This paragraph was written just to demonstrate relative different in power between the CPW and microstrip designs, the exact method used to estimate the noise power is not important for this purpose. The suggested method can be used as well, but the conclusion remains the same.

Page 25, right column, line 2 from bottom. "...but in order to minimize cross talk..." cross talk issue is not discussed in this paper. It is suggested to add analysis on cross talk, which will be interesting.
Response: This is unfortunately beyond the scope of the paper, but I understand that it is important for other applications such as SIS mixers, which again is not the focus of this paper.

Competing Interests: No competing interests were disclosed.

Reviewer Report 15 August 2022

https://doi.org/10.21956/openreseurope.16055.r29724

?

Fausto Patricio Mena
[1] Electrical Engineering Department, University of Chile, Santiago, Chile
[2] National Radio Astronomy Observatory, Charlottesville, VA, USA

The work describes interesting methods and simulations for the implementation of Kinetic Inductance Travelling Wave amplifiers. There are three clear parts in the paper.

1. The first part presents an improvement in the Coupling Equations to model parametric amplifiers. Although the improvement seems to be intuitively correct, no clear justification is stated. Similar work towards modeling the effect of losses in parametric amplifiers have not been cited (https://www.nrao.edu/meetings/isstt/papers/2019/2019063066.pdf).

2. The second part presents a meticulous study for finding and optimizing the most appropriate superconducting material suitable for implementing parametric amplifiers. This section is well written and very interesting insights are presented.

3. The last part presents several designs and simulations for future implementations of parametric amplifiers. Although the results are encouraging, my impression is that the authors are over-interpreting their findings. They have to be more careful when stating and drawing conclusions from simulations that have not been tested experimentally. Moreover, there is a stark contrast with the other sections, it needs a careful grammatical and spelling review.

The work, although interesting, it is rather lengthy and my recommendation is that the authors have to make more effort in shortening it, especially in Section 5. Sometimes the descriptions are repetitive. After presenting the first configuration, the other configurations do not need to be over-lengthy described since much of the findings are rather similar.

More specific comments are given in the accompanying document. (Boon-Kok Tan comments.pdf)

Is the work clearly and accurately presented and does it cite the current literature?
Partly

Is the study design appropriate and does the work have academic merit?
Yes

Are sufficient details of methods and analysis provided to allow replication by others?
Yes

If applicable, is the statistical analysis and its interpretation appropriate?
Not applicable

Are all the source data underlying the results available to ensure full reproducibility?
Yes

Are the conclusions drawn adequately supported by the results?
Partly

Competing Interests: I have been working in a very similar line of research and have used similar methods. This has not affected my ability to provide an impartial review for this article.

I confirm that I have read this submission and believe that I have an appropriate level of expertise to confirm that it is of an acceptable scientific standard, however I have significant reservations, as outlined above.

Author Response 01 Sep 2023

Boon Kok Tan

Dear Prof. Mena, Thank you for taking your time to review the article thoroughly. My sincere apology for the long delay in responding. The responses for all your very useful comments are as below: The work describes interesting methods and simulations for the implementation of Kinetic Inductance Travelling Wave amplifiers. There are three clear parts in the paper.

1. The first part presents an improvement in the Coupling Equations to model parametric amplifiers. Although the improvement seems to be intuitively correct, no clear justification is stated. Similar work towards modeling the effect of losses in parametric amplifiers have not been cited (https://www.nrao.edu/meetings/isstt/papers/2019/2019063066.pdf).

   Response: Thanks for the suggestion. Citation added.

2. The second part presents a meticulous study for finding and optimizing the most appropriate superconducting material suitable for implementing parametric amplifiers. This section is well written and very interesting insights are presented.

   Response: Thanks.

3. The last part presents several designs and simulations for future implementations of parametric amplifiers. Although the results are encouraging, my impression is that the authors are over-interpreting their findings. They have to be more careful when stating and drawing conclusions from simulations that have not been tested experimentally. Moreover, there is a stark contrast with the other sections, it needs a careful grammatical and spelling review.

   Response: This paper focuses on the design considerations of KITWPA from the perspective of electromagnetism mainly, hence all the conclusions were made referring to the simulations done with rigorous mathematical frameworks, not via experimental results which certainly would have to include even more subtle effects such as fabrication defects etc, which would be beyond the scope of this paper. We toned done the 'over-interpretation', nevertheless, in the updated version as suggested.

The work, although interesting, it is rather lengthy and my recommendation is that the authors have to make more effort in shortening it, especially in Section 5. Sometimes the descriptions are repetitive. After presenting the first configuration, the other configurations do not need to be over-lengthy described since much of the findings are rather similar.

Response: The updated manuscript has been shortened.

More specific comments are given in the accompanying document. (Boon-Kok Tan comments.pdf) The responses were given in the pdf.

Competing Interests: No competing interests were disclosed.